MICROBIOLOGY

An intramolecular cross-talk in D29 mycobacteriophage endolysin governs the lytic cycle and phage-host population dynamics

Gokul Nair and Vikas Jain*

D29 mycobacteriophage encodes LysA endolysin, which mediates mycobacterial host cell lysis by targeting its peptidoglycan layer, thus projecting itself as a potential therapeutic. However, the regulatory mechanism of LysA during the phage lytic cycle remains ill defined. Here, we show that during D29 lytic cycle, structural and functional regulation of LysA not only orchestrates host cell lysis but also is critical for maintaining phage-host population dynamics by governing various phases of lytic cycle. We report that LysA exists in two conformations, of which only one is active, and the protein undergoes a host peptidoglycan–dependent conformational switch to become active for carrying out endogenous host cell lysis. D29 maintains a pool of inactive LysA, allowing complete assembly of phage progeny, thus helping avoid premature host lysis. In addition, we show that the switch reverses after lysis, thus preventing exogenous targeting of bystanders, which otherwise negatively affects phage propagation in the environment.

INTRODUCTION

Despite decades of research, mycobacteria-associated diseases like tuberculosis continue to be the leading causes of death, especially in the developing countries (1, 2). Several drugs are available that target mycobacterial cell wall biosynthesis, DNA replication, RNA and protein synthesis, and other metabolic pathways (3, 4). However, only a handful of drugs are able to efficiently surpass the mycobacterial cell wall (5, 6). The complex and robust nature of mycobacterial cell wall is the main reason behind such low permeability for these drugs (7). Peptidoglycan (PG) being a major component of the cell wall, plays a crucial role in maintaining the structural integrity of the cell by regulating shape, elongation, and cell division, which also makes it a prime drug target to tackle mycobacterial infection (8). PG is a complex heteropolymer consisting of long glycan strands of N-acetyl muramic acid (NAM) and N-acetyl glucosamine (NAG), linked by β-1,4 glycosidic bonds. However, several modifications such as the presence of a mixture of both the typical NAM and its hydroxylated derivative, N-glycolyl muramic acid (MurGlyc) have been observed with mycobacterial PG, which possibly form additional hydrogen bonds to provide additional strength to the PG (9). The glycan chains are cross-linked by short peptide bridges, which vary in bacterial groups (8, 10). The pentapeptide consists of L-Ala, D-isoglutamate (D-iso Glu), meso-diaminopimelate (m-DAP), D-Ala, and D-Ala. However, modifications such as amidation of the free carboxylic acids of D-iso Glu, m-DAP, and the terminal D-Ala have been observed in mycobacteria (9). These pentapeptides exhibit 3 → 3 linkages between two m-DAP residues in mycobacteria instead of 3 → 4 m-DAP to D-Ala linkages present in other bacteria. Mycobacteria have much more peptide cross-links, which create a more compact and meshy PG architecture, thus harboring higher mechanical strength than others (9). Drugs such as cycloserine and β-lactams have been used to inhibit mycobacterial PG biosynthesis (11, 12). However, lack of efficient PG-hydrolyzing

drugs along with increase in pathogenic graph of multidrug- resistant, extreme drug-resistant, and total drug-resistant strains of *Mycobacterium tuberculosis* have resulted in an urgent need for alternative therapeutic candidates (13–15).

Virulent phages due to their ability to lyse host bacteria have long been considered as potential candidate to eliminate drug-resistant bacteria (16). Their ability to lyse host cells is endowed by phage-encoded endolysin, which targets host PG to release phage progeny (17, 18). However, a poor understanding of the regulatory mechanism of these endolysins and their mode of action lead to failure in developing them as effective therapeutic candidates (19). Therefore, there is a need to have a comprehensive understanding of the structure, function, and regulation of these endolysins, which will allow a rational engineering of these proteins to develop them as effective therapeutics.

Usually, phages infecting Gram-negative bacteria encode endolysins, which are globular in nature, while phages infecting Gram-positive have modular endolysin, which usually is composed of single catalytic domain and cell wall binding domain (20–22). D29 mycobacteriophage LysA endolysin was shown to harbor two catalytic domains, namely, an N-terminal domain (NTD) and a lysozyme-like domain (LD), in addition to a C-terminal cell wall binding domain (CTD) (23–25). The multidomain architecture of endolysin usually provides structural and functional flexibility to regulate host cell lysis in a controlled and an efficient manner (26). However, a lack of structural characterization makes it difficult to draw any conserved structural inferences to understand how these endolysins function and regulate host cell lysis.

In this study, we examined the role of CTD in facilitating D29 LysA to exploit its modular nature to gain structural and functional plasticity required at different stages of host cell lysis. We also decoded the significance of LysA regulation in maintaining the phage-host equilibrium in the environment by governing lytic cycle. There has been a lack of understanding regarding the regulation of LysA. Thus, a deep structural and functional insight into LysA will allow us to engineer a stable, effective, and proficient enzyme-based therapeutic candidate against mycobacterial infection.

Microbiology and Molecular Biology Laboratory, Department of Biological Sciences, Indian Institute of Science Education and Research (IISER), Bhopal 462066, Madhya Pradesh, India.
*Corresponding author. Email: vikas@iiserb.ac.in

RESULTS

LysA maintains an inactive closed conformation in the absence of host substrate

We previously reported that LysA even after fusing with secretory signal sequence did not elucidate cell lysis in noncanonical host such as *Escherichia coli* (*23*), indicating the existence of a precise regulatory mechanism in LysA. Here, we deciphered how modular architecture of LysA provides structural and functional plasticity required to regulate its activity.

Structure prediction of LysA from GalaxyWEB server yielded two distinct conformations of the protein, which we here refer to as "close" and "open" conformations (Fig. 1A). Both the conformations were found to harbor clearly identifiable domains (NTD, LD, and CTD), interconnected with linker regions. At this juncture, we postulated that these two conformations may interconvert to regulate protein's activity, as has been suggested for many other proteins (*19*). Thus, we hypothesized that the open and close conformations represent active and inactive LysA, respectively. The predicted structure with close conformation retained its structural conformation (Fig. 1B) even after a 200-ns molecular dynamics (MD) simulation (MDS). In addition, MDS data showed no notable variation in either root mean square deviation (RMSD) or root mean square fluctuation (RMSF) suggesting it to be a stable conformation (fig. S1).

To further confirm our hypothesis, we performed Förster resonance energy transfer (FRET), which allowed us to examine domain movements. Several LysA variants having two Cys residues (Table 1) were generated to install fluorescent probe in the protein by attaching it to a free thiol offered by the cysteine. However, we were able to purify only LysA$^{Cys17-427}$ and LysA$^{Cys115-427}$ without compromising protein's solubility and activity (Fig. 1C). Both of the purified LysA variant proteins showed PG hydrolytic activity similar to the wild-type (WT) LysA, suggesting no loss of function (Fig. 1D). Far–ultraviolet (UV) circular dichroism (CD) data of LysA Cys variants showed no notable differences among the WT LysA and the mutated proteins (Fig. 1E). We next labeled both LysA Cys variants with fluorescent probes 1,5-IAEDANS [5-({[(2-iodoacetyl) amino] ethyl} amino) naphthalene-1-sulfonicacid] as donor and 6-IAF (6-iodoacetamidofluorescein) as acceptor following established protocols (*27, 28*). FRET was monitored by exciting the labeled proteins with the donor's excitation wavelength (336 nm) and recording the emission spectra from 360 to 600 nm. Fluorescence spectra of both the proteins showed the emission profile of IAF, with no considerable emission of IAEDANS (Fig. 1F). Similar results were obtained with another set of probes viz. 6-IAF (donor) and QSY-9 (quencher). Here, we observed reduced IAF emission upon excitation with 494-nm wavelength; which suggests quenching of IAF emission (fig. S2). Such drastic reduction in donor emission in the presence of acceptor or quencher due to FRET suggests close proximity of both fluorophores, which is achievable only in close conformation of LysA. This further corroborates with our MDS data.

Our data above suggest that interaction between NTD and CTD is crucial for maintaining close conformation in LysA. Thus, to understand the significance of maintaining a stable close conformation, we disrupted this conformation by generating a CTD-deleted variant of LysA (LysA^{ΔCTD}) and carried out its expression studies with green fluorescent protein (GFP)–tagged protein in *Mycobacterium smegmatis* (Msm) cells from an acetamide-inducible promoter (Fig. 1G). However, because it is difficult to monitor such small growth deficit in

induced condition, we carried out the growth curve in uninduced conditions. This promoter is known to give leaky expression in the absence of acetamide (*29*), and, therefore, it allowed us to perform our studies at low expression level. LysA-GFP showed substantially less retarded mycobacterial cell growth in the absence of acetamide in comparison to LysA^{ΔCTD}-GFP (Fig. 1G). The presence of protein in the supernatant of the harvested cells is an indicator of host cell lysis due to the protein being translocated to the target site (PG). To examine this further, we measured the release of GFP-tagged proteins in the culture supernatant with time. Our fluorescence data suggest slow LysA-GFP release in the culture supernatant, indicating slow translocation of LysA to the target site as compared to LysA^{ΔCTD} (Fig. 1H). The delay in LysA release contributes to an inconsiderable reduction in Msm growth, whereas rapid release of LysA^{ΔCTD} evokes substantial reduction in Msm growth, thus suggesting that disruption of close conformation due to CTD deletion brings enzyme in an active form. Furthermore, our GFP release assay indicates no major difference in the expression levels of all the proteins in the Msm cells (fig. S3). The difference in the measured fluorescence in the culture supernatant, therefore, is a result of slow translocation of LysA to the target site and not due to the differential expression of proteins. Together, slow translocation and activity by WT LysA protein suggest that LysA likely maintains an inactive state until the time it interacts with the host PG due to the intact close conformation as seen in MDS data.

LysA exhibits two distinct host substrate–dependent functional states

To address LysA activation in the presence of host substrate, we subjected the close conformation of LysA to MDS in presence of PG components NAM-NAG-NAM. We observed a conformational switch from close to open in this simulation (Fig. 2A). Visualization of all the frames of MDS suggested that the interaction of substrate with CTD induces the conformational change in LysA, which likely allows the catalytic domains to access host substrate (fig. S4). We, therefore, propose that a close-to-open conformational switch in the presence of host substrate is essential for the protein to become catalytically active. Furthermore, RMSF calculation of each residue indicated extensive fluctuations in CTD, especially in the linker region between LD and CTD (fig. S5), suggesting that the linker region provides the much-needed flexibility to LysA to undergo conformational switch. To further examine the interconversion of conformational states, we performed FRET experiments with IAEDANS and IAF-labeled LysA$^{Cys17-427}$ and LysA$^{Cys115-427}$, treated with different amounts of Msm PG (PG^{Msm}). Both the variants in the presence of PG^{Msm} showed a clear shift in the emission spectra i.e., an increase in IAEDANS emission and a concomitant decrease in IAF emission, when excited at 336 nm (Fig. 2, B to D). However, no such shift was observed in the absence of PG^{Msm}. A shift in the emission spectra indicates loss of FRET in the presence of PG^{Msm}, which validates our in silico observation of host substrate–induced switch between close and open conformations.

We also performed similar experiments with *E. coli* PG (PG^{Eco}) to assess whether the conformational switch–based regulation is driven only by the canonical host (Msm) PG (Fig. 2, E to G). No substantial change in the fluorescence spectra was observed in the presence or absence of PG^{Eco}, which confirmed the role of substrate specificity in LysA conformational switch.

Similar results were obtained with IAF (donor)–QSY-9 (quencher)–labeled proteins, where an increase in donor emission was observed
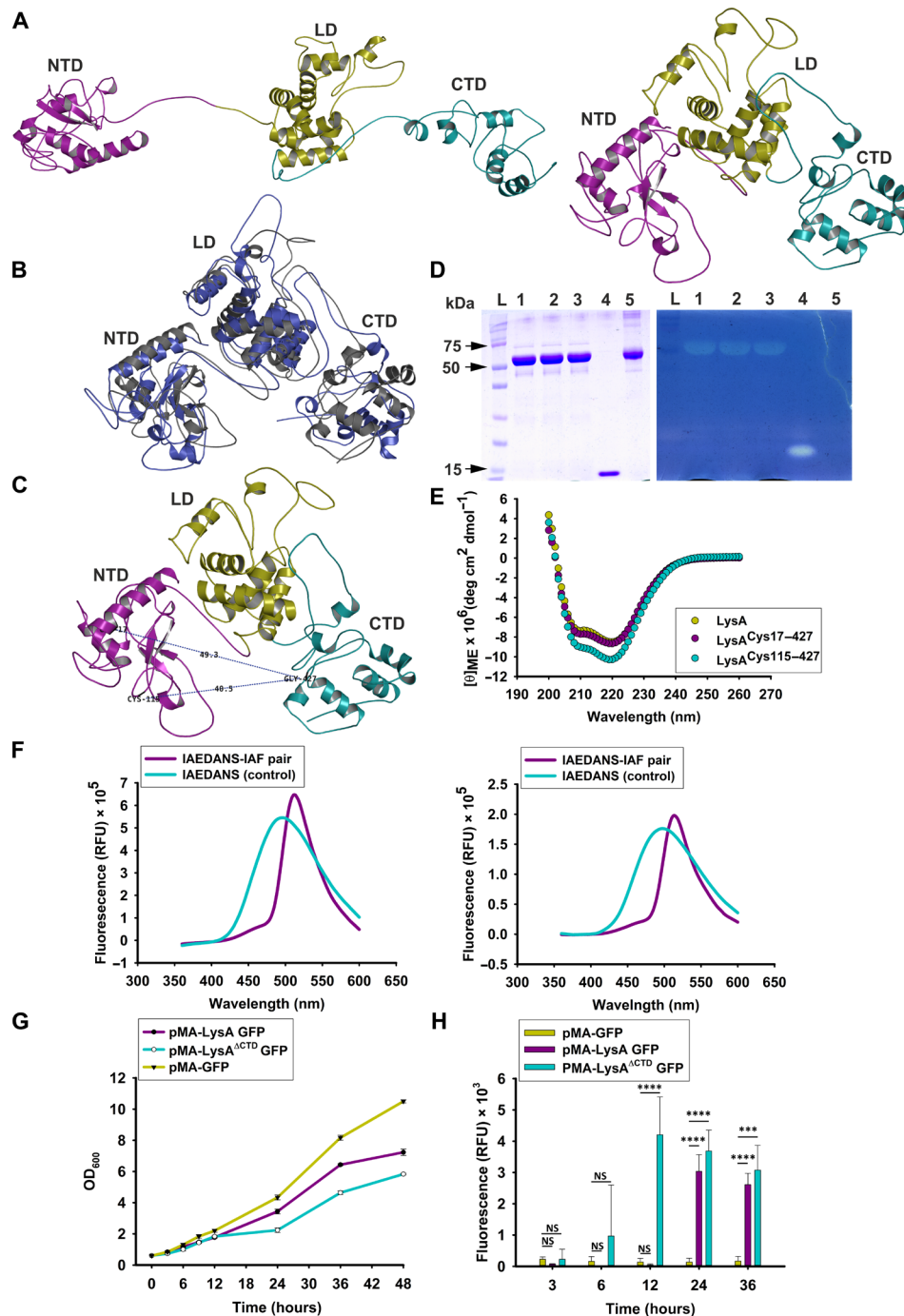
Fig. 1. Structural insights into the inactive state of LysA protein. (**A**) Visualization of predicted LysA structure showing two distinct: open (left) and closed (right) conformations. (**B**) Structural alignment of predicted LysA structure having close conformation with the structure obtained after MDS. (**C**) Mapping of residues selected to generate cysteine pairs used for experimental studies. Residues of WT LysA at 17, 115, and 427 are represented with their estimated distances with each other. (**D**) Zymography assay showing PG hydrolytic activity of LysA and its Cys variants. Lanes from left to right represent WT LysA, LysA$^{Cys17-427}$, LysA$^{Cys115-427}$, lysozyme, and bovine serum albumin (BSA). Left panel shows the loading control, and the right panel shows zymography gel image. "L" represents molecular weight ladder. (**E**) Representative far-UV CD spectrum of LysA (yellow), LysA$^{Cys17-427}$ (magenta), and LysA$^{Cys115-427}$ (cyan). Data are shown in molar ellipticity. LysA and its Cys variants do not show any notable structural differences. (**F**) Fluorescence measurement of LysA cysteine variants LysA$^{Cys17-427}$ (left) and LysA$^{Cys115-427}$ (right) labeled with both IAEDANS (donor) and IAF (acceptor) upon excited with 336 nm. The emission was recorded from 360 to 600 nm covering both IAEDANS and IAF emissions. IAEDANS mono-labeled protein is used as control. (**G**) Growth curve of Msm cells with low expression of LysA-GFP (magenta), LysA$^{\Delta CTD}$-GFP (cyan), and GFP as control (yellow) monitored every 3 hours. The data at each time point represent an average of measurements performed in triplicate; error bars denote SD. (**H**) GFP release of growth curve samples [presented in (G)] was recorded in the supernatant collected at every time point; data represent an average of measurements performed in triplicate, and error bars denote SD. P value analysis: ****$P < 0.0001$; ***$P < 0.0005$; NS, not significant, when the activity of LysA-GFP and LysA$^{\Delta CTD}$-GFP compared with GFP control; RFU, relative fluorescence unit.

Table 1. List of LysA protein cysteine variants generated for FRET experiments. A "✓" represents the presence of a particular mutation at that respective position in the LysA construct. The numbers indicate the position of the amino acid in the full-length WT protein.

S. No.	Cysteine pairs	Cys to Ser				Ser to Cys		Gly to Cys		Glu to Cys
		17	41	115	212	3	138	427	441	498
1.	Cys17–427		✓	✓	✓			✓		
2.	Cys17–441		✓	✓	✓				✓	
3.	Cys17–498		✓	✓	✓					✓
4.	Cys41–427	✓		✓	✓			✓		
5.	Cys41–441	✓		✓	✓				✓	
6.	Cys41–498	✓		✓	✓					✓
7.	Cys115–427	✓	✓		✓			✓		
8.	Cys115–441	✓	✓		✓				✓	
9.	Cys115–498	✓	✓		✓					✓
10.	Cys212–427	✓	✓	✓				✓		
11.	Cys212–441	✓	✓	✓					✓	
12.	Cys212–498	✓	✓	✓						✓
13.	Cys3–427	✓	✓	✓	✓	✓		✓		
14.	Cys3–441	✓	✓	✓	✓	✓			✓	
15.	Cys3–498	✓	✓	✓	✓	✓				✓
16.	Cys138–427	✓	✓	✓	✓		✓	✓		
17.	Cys138–441	✓	✓	✓	✓		✓		✓	
18.	Cys138–498	✓	✓	✓	✓		✓			✓

upon PG^{Msm} addition, whereas no such increase occurred upon PG^{Eco} addition (fig. S6). The diluted samples also showed results similar to the undiluted ones, thus confirming that the observed FRET was due to an intramolecular, and not intermolecular, cross-talk between the domains (fig. S6).

Our MDS and FRET data along with growth curve (Fig. 1H) further establish that LysA maintains an inactive (close conformation) state inside the host cytoplasm and undergoes a conformational switch to an active (open conformation) state only in the presence of host PG, which is required for its activity.

Arginine-rich CTD of LysA is essential for a stable interaction with the host PG

We previously demonstrated that CTD shows specific and stable interaction with mycobacterial PG (23, 25). However, while CTD is not essential for the functioning of catalytic domains, our data presented above demonstrate that (i) CTD is involved in regulating LysA activity and (ii) it makes LysA host specific. Thus, structural insight into CTD interaction with PG is a prerequisite to decode the role of CTD in LysA-mediated host cell lysis. We, therefore, predicted structure of CTD using QUARK server (30), screened them using SAVES server (31), and subjected it to MDS to obtain a stable conformation (fig. S7).

We then performed MDS of CTD docked with PG components (NAG and NAM); the docking was carried out by PyRx virtual screening tool (32). We performed multiple rounds of sequential docking and simulations to saturate CTD's ligand binding capacity, thereby mimicking a realistic scenario of the bacterial PG exhibiting long chain of NAG-NAM as substrate for CTD (figs. S8 to S10). Our simulation data revealed the involvement of multiple arginines in facilitating CTD's interaction with its substrate (Fig. 3A). Arg is one of the most abundant amino acids across cell wall binding domains of lysins, which show sequence similarity with D29 LysA (fig. S11, A and B). This immediately suggests the significance of an arginine-rich profile of CTD in providing affinity toward bacterial PG.

To further investigate the importance of arginines in CTD-PG interaction, we carried out alanine substitutions of Arg present in CTD in groups of two or three residues, depending on their proximity in the sequence, and generated a library of mutated CTD proteins (fig. S11C and Table 2). PG^{Msm} binding assay carried out with these mutants demonstrated that while two groups of Arg-to-Ala substituted proteins viz. R5+6 and R6+7 (Table 2) showed a substantial reduction in PG binding, one mutant R5+6+7 (Table 2) showed complete loss of binding to PG^{Msm} (Fig. 3B and fig. S12). Similarly, fluorescence-based Msm cell binding assays with GFP-tagged CTD carrying these mutations also concurred with the loss of function observed in PG binding assay (Fig. 3C). In line with the architecture of the PG layer, our data indicate that the interaction of multiple arginines with PG plays a crucial role in stabilizing LysA interaction with the host PG. Furthermore, far-UV CD (fig. S13) and structural alignment (fig. S14) of these mutants with WT CTD confirm that their inability to bind PG^{Msm} is not due to a structural change in the protein.

To further dissect the role of CTD in regulating dual functional state of LysA, we carried out FRET experiments with IAEDANS/IAF-labeled LysA Cys variants ($LysA^{Cys17-427}*CTD$ and $LysA^{Cys115-427}*CTD$)
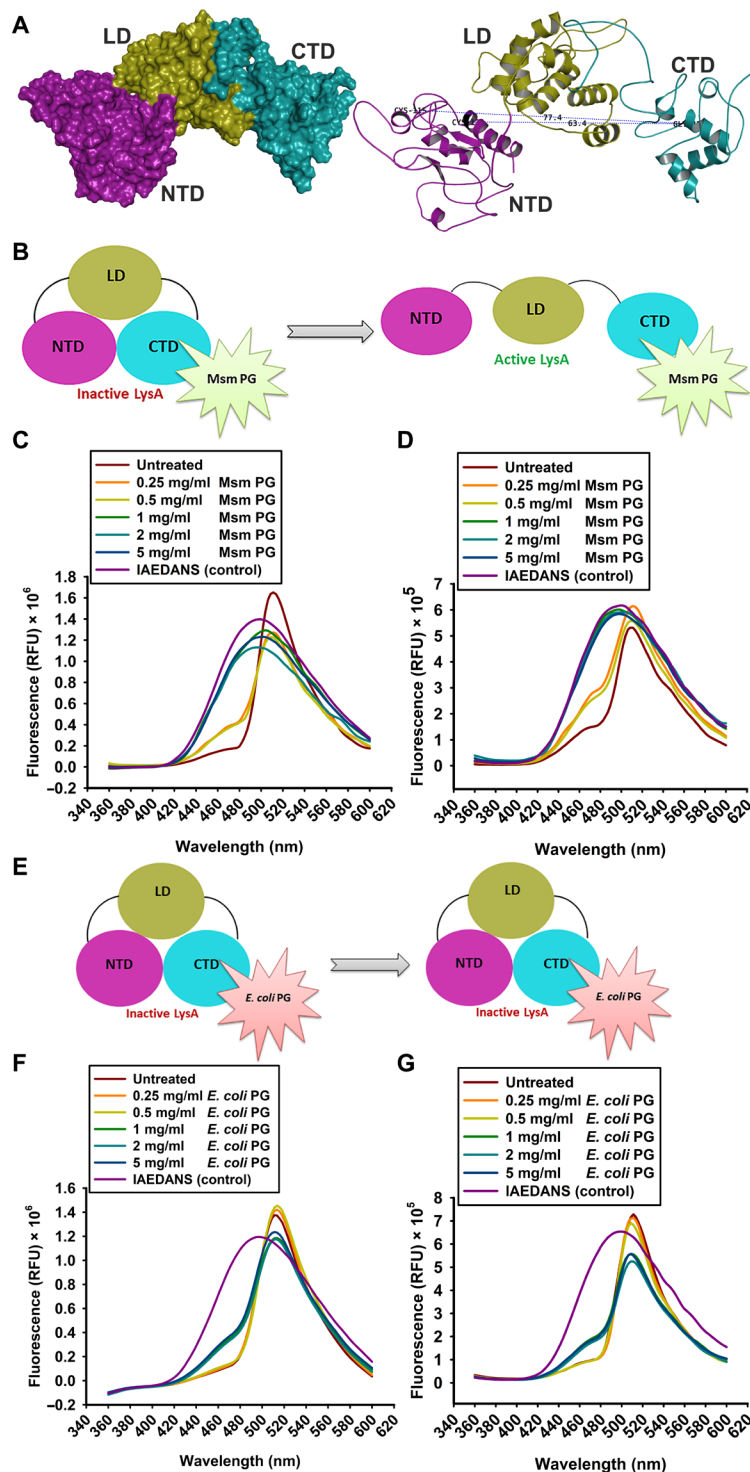
Fig. 2. Effect of canonical and noncanonical host PG on the structural conformation of LysA protein. (**A**) Visualizing MDS of LysA protein in the presence of PG components. LysA protein attains open conformation upon interaction with PG components, NAM-NAG-NAM. (**B**) Schematic representation of *Mycobacterium smegmatis* PG (Msm PG) induced conformational switch shown by LysA protein. Fluorescence measurement of LysA$^{Cys17–427}$ (**C**) and LysA$^{Cys115–427}$ (**D**) proteins labeled with both IAE-DANS and IAF upon treatment with different concentrations of Msm PG. (**E**) Schematic representation showing effect of PG from noncanonical host (*E. coli*) on LysA protein conformation. Fluorescence measurement of LysA$^{Cys17–427}$ (**F**) and LysA$^{Cys115–427}$ (**G**) proteins labeled with both IAEDANS and IAF upon treatment with different concentrations of *E. coli* PG. In (C), (D), (F), and (G), fluorescence was recorded by exciting the sample at 336 nm (donor wavelength) and emission was recorded in the range of 360 to 600 nm covering both IAEDANS and IAF emissions. IAEDANS mono-labeled protein is used as control in the experiments.
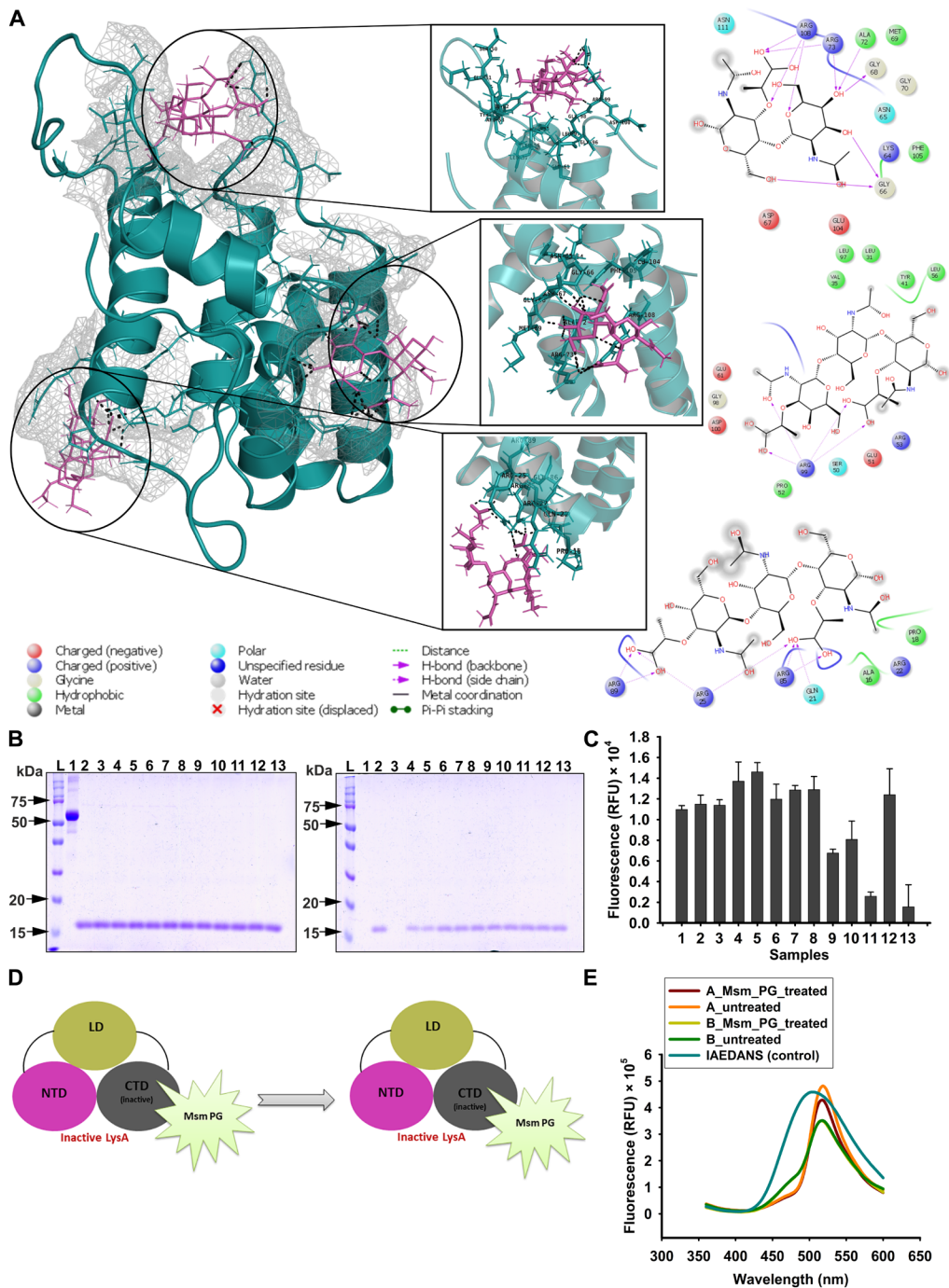
Fig. 3. Interaction of CTD with host PG. (**A**) MDS data showing CTD (cyan) interacting with PG components NAG and NAM (magenta). CTD interacting surface with its substrate is represented as gray mesh over the structure. Detailed interaction is shown with a two-dimensional interaction map on the right-side panel, with multiple arginine residues facilitating CTD interaction with PG components. (**B**) PG binding assay showing binding of CTD protein harboring arginine mutation with Msm PG. Left panel shows loading control, whereas the right panel shows bound protein. Lanes 1 and 2 in both panels represent BSA and WT CTD, respectively. Lanes 3 to 13 represent CTD harboring R5+6+7, R6+7, R5+6, R8, R7, R6, R5, R4, R3, R2, and R1 mutations (list of these mutations along with abbreviation and respective positions are provided in Table 2). L represents molecular weight marker with few bands marked. (**C**) Fluorescence-based Msm cell binding assay showing binding of CTD-GFP protein harboring arginine mutation with Msm cells. Samples 1 to 11 represent CTD-GFP protein harboring R1, R2, R3, R4, R5, R6, R7, R8, R5+6, R6+7, R5+6+7, respectively, while samples 12 and 13 represent CTD-GFP and BSA, respectively. Data represent an average of measurements performed in triplicate; error bars denote SD. (**D**) Schematic showing LysA with inactive CTD. Here, CTD in LysA harbors R5+6+7 mutations, rendering CTD incapable of binding to mycobacterial PG. Hence, it displays no loss of FRET even in the presence of Msm PG, suggesting role of CTD in host substrate–induced conformational switch. (**E**) FRET measurements of LysA cysteine variants with inactive CTD (A, LysA$^{Cys17–427}$*CTD; B, LysA$^{Cys115–427}$*CTD) labeled with IAEDANS and IAF upon treatment with Msm PG. Fluorescence was recorded by exciting sample at 336 nm (donor wavelength), and emission was recorded from 360 to 600 nm. IAEDANS mono-labeled protein is used as control.

Table 2. List of Arg-to-Ala substitutions carried out in CTD of LysA along with their abbreviations used in the present study.

Abbreviation	Gene and domain	Mutation	Positions
R1	GP10, CTD	Arg to Ala	22, 25
R2	GP10, CTD	Arg to Ala	53
R3	GP10, CTD	Arg to Ala	73
R4	GP10, CTD	Arg to Ala	80
R5	GP10, CTD	Arg to Ala	85, 89, 92
R6	GP10, CTD	Arg to Ala	99, 101
R7	GP10, CTD	Arg to Ala	108, 110
R8	GP10, CTD	Arg to Ala	130
R5+6	GP10, CTD	Arg to Ala	85, 89, 92, 99, 101
R6+7	GP10, CTD	Arg to Ala	99, 101, 108, 110
R5+6+6	GP10, CTD	Arg to Ala	85, 89, 92, 99, 101, 108, 110

harboring the R5+6+7 mutations, which made CTD unable to bind PG^{Msm} (Fig. 3, D and E). Far-UV CD profile of both variants showed no considerable structural changes in the proteins due to mutations (fig. S15). Only IAF emission was observed in this fluorescence spectrum even after adding PG^{Msm} (Fig. 3, D and E), suggesting that host PG–induced conformational switch no longer occurs in LysA harboring inactive CTD. Together, our data establish that recognition of host PG by CTD induces the conformational switch in LysA, which is required to activate the enzyme for PG hydrolysis. Thus, LysA harboring a CTD domain, which is incapable of recognizing and binding to host PG, displays loss of catalytic function, i.e., PG hydrolysis. This loss in activity is due to the inhibition of CTD-mediated conformational switch (close to open), which is essential for the catalytic activity of LysA.

CTD regulates LysA-mediated endogenous and exogenous host cell lysis

To further understand the importance of CTD in regulating LysA-mediated host cell lysis, we expressed both WT LysA and LysA$^{\Delta CTD}$ in WT Msm (Fig. 4A). Unexpectedly, expression of LysA$^{\Delta CTD}$ showed a steep decline in host mycobacterial cell population as compared to LysA. Alamar blue cell viability assay data further validate that LysA$^{\Delta CTD}$ triggered a rapid endogenous host cell lysis (Fig. 4B).

Because LysA targets PG layer of mycobacterial cell wall, we next studied the alteration in cell morphology (*33*) to assess the impact of enzyme on the host bacterium. Our experiments show that "mild" expression (induction by 0.1% acetamide) of LysA and LysA$^{\Delta CTD}$ affects Msm colony morphology considerably, indicating an alteration in cell wall (Fig. 4C). However, Congo red dye–binding and sliding motility data clearly indicate that the extent of Msm cell wall alteration is more remarkable when LysA$^{\Delta CTD}$ is expressed (Fig. 4C). Hence, we asked whether and how CTD deletion affects LysA translocation to periplasm, which is crucial for PG targeting. To address this, we expressed LysA and LysA$^{\Delta CTD}$ carrying GFP at either terminus in Msm; GFP alone was used as control (Fig. 4D). LysA$^{\Delta CTD}$ showed an acute polar localization with no cytoplasmic accumulation like GFP. In contrast, LysA showed somewhat lesser polar localization with a clear presence in cytoplasm (Fig. 4D). As seen in LysA, mycobacterial PG remodeling enzymes also exhibit similar polar

localization for PG rearrangement during cell division (*34*), suggesting that LysA might be a host-acquired gene during the course of evolution; this, however, requires further exploration.

The microscopy data and slow release of LysA protein observed in the supernatant of previous expression studies (Fig. 1H) further verify the slower translocation of LysA compared to LysA$^{\Delta CTD}$. Together, they confirm that LysA maintains an inactive (close) state inside host cytoplasm, which then undergoes a conformation switch to an active (open) state. This conformational regulation causes a delay in the translocation of LysA to the periplasmic space. In addition, a failure to evoke comparatively less effect on mycobacterial cells upon low expression (Fig. 1G) suggests that the protein is indeed maintained in an inactive state and gradually translocated to the target site. Meanwhile, in the case of LysA$^{\Delta CTD}$ protein, the close (inactive) conformation as seen with LysA is disrupted because of the deletion of CTD. Thus, LysA$^{\Delta CTD}$ protein remains in an active (open) state and does not require any conformational switch for its activation. LysA$^{\Delta CTD}$ protein immediately gets translocated to the periplasmic space because of the absence of conformational regulation, which even in a low-expression state evokes a considerable effect on the Msm population. This also suggests that the catalytic domains of LysA can carry out PG hydrolysis even in the absence of CTD.

The absence of conformational regulation with LysA$^{\Delta CTD}$ is the reason why we have observed contrastingly different results in the case of LysA devoid of CTD (LysA$^{\Delta CTD}$) and LysA harboring CTD with Arg-to-Ala substitutions (R5 + 6 + 7), which inhibits binding of CTD to host PG. Only LysA with these mutations displays a loss of PG hydrolytic activity, while the truncated LysA$^{\Delta CTD}$ protein retains its PG hydrolytic activity.

MDS of substrate-induced open conformation of LysA after ligand removal led to reversal of the conformational switch, and the protein regained its close inactive conformation (Fig. 5A and fig. S16). Such reversal of conformational switch in the absence of substrate intrigued us to ask what happens to the LysA after host cell lysis. To address this, we monitored the growth of a mixed culture of Msm with two types of cells: the producer cell, i.e., Msm cell expressing either LysA or LysA$^{\Delta CTD}$, and the bystander cells, i.e., Msm cells expressing either GFP or empty vector (Fig. 5B and fig. S17A). Upon expression of these proteins in the presence of acetamide, the producer cells lyse,
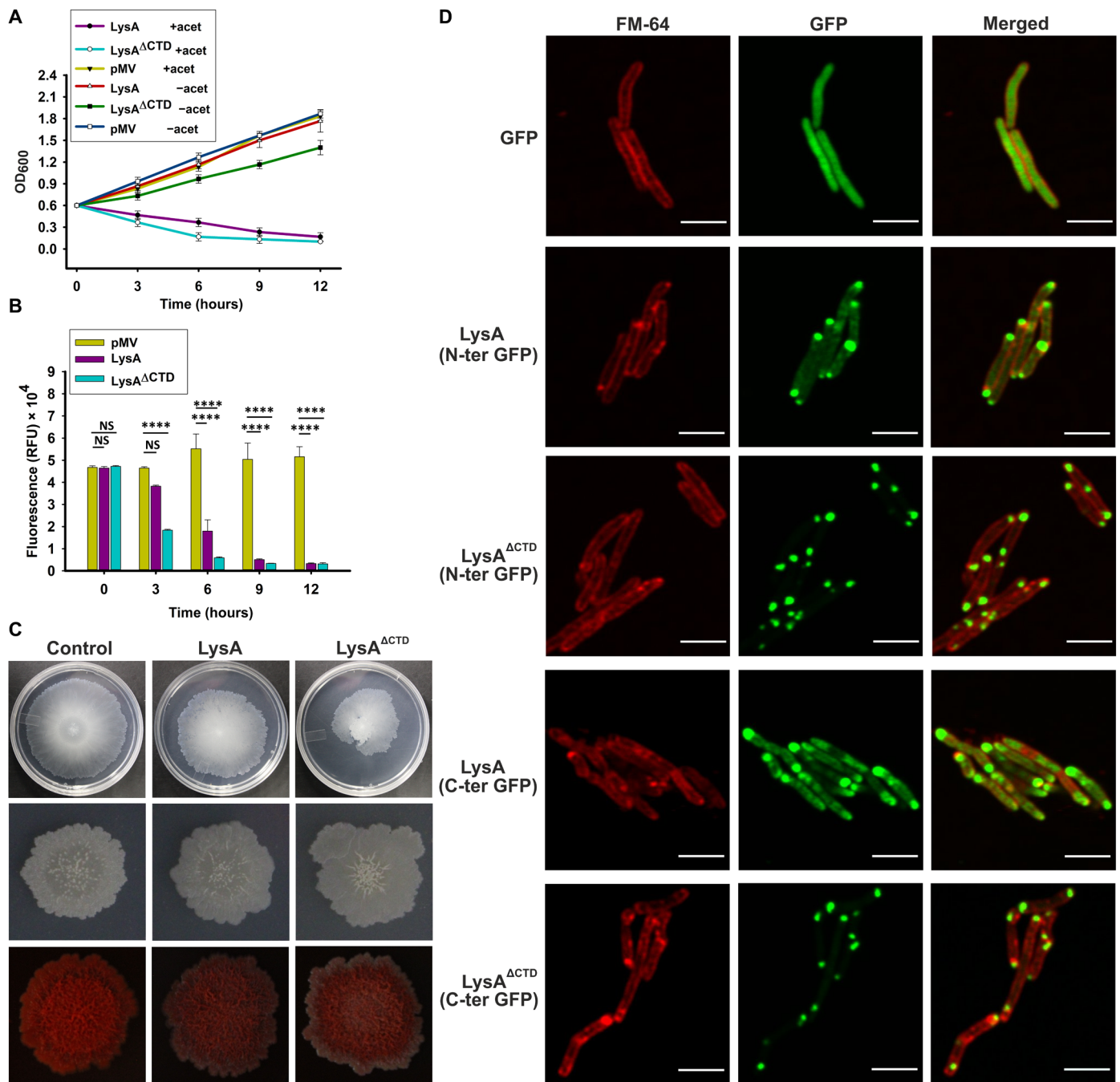
Fig. 4. Significance of CTD in LysA mediated endogenous host cell lysis. (**A**) The growth of Msm cells expressing either LysA or LysA$^{\Delta CTD}$ was observed by measuring OD$_{600}$ after induction with 0.2% acetamide (+acet); "−acet" represents absence of inducer. (**B**) Alamar blue assay was performed to measure the proportion of viable cells. In both (A) and (B), the data at each time point represent an average of measurements performed in triplicate; the error bars denote the SD. In (B), *P* value analysis: ****P < 0.0001; NS, not significant, when the activity of LysA and LysA$^{\Delta CTD}$ compared with control. (**C**) Phenotypic characterization of Msm cells with mild expression of LysA and LysA$^{\Delta CTD}$ along with empty vector (control), carried out by monitoring sliding motility (top), colony morphology on MB agar plate (middle), as well on Congo red agar plate (bottom). LysA$^{\Delta CTD}$ shows substantial alteration in colony morphology and reduction in sliding motility as compared to LysA. (**D**) Live cell fluorescence microscopy of Msm cells expressing LysA and LysA$^{\Delta CTD}$ protein tagged with GFP. GFP without a gene of interest was used as control in the experiment. Cells were counterstained with FM4-64 dye to visualize the cell envelope. Panels from top to bottom represent Msm cells expressing GFP, LysA having GFP at its N terminus, LysA$^{\Delta CTD}$ with N-terminal GFP, LysA with C-terminal GFP, and LysA$^{\Delta CTD}$ with C-terminal GFP, respectively. Here, we positioned GFP at either terminus to rule out the possibility of the effect of tag position on the secretion of protein. Scale bar represents 3 μm in each panel. GFP showed complete cytoplasmic localization suggesting no periplasmic secretion. However, LysA$^{\Delta CTD}$ shows precise polar localization, whereas LysA shows clear evidence of cytoplasmic presence along with mild polar localization, suggesting slow protein translocation toward the cell wall.
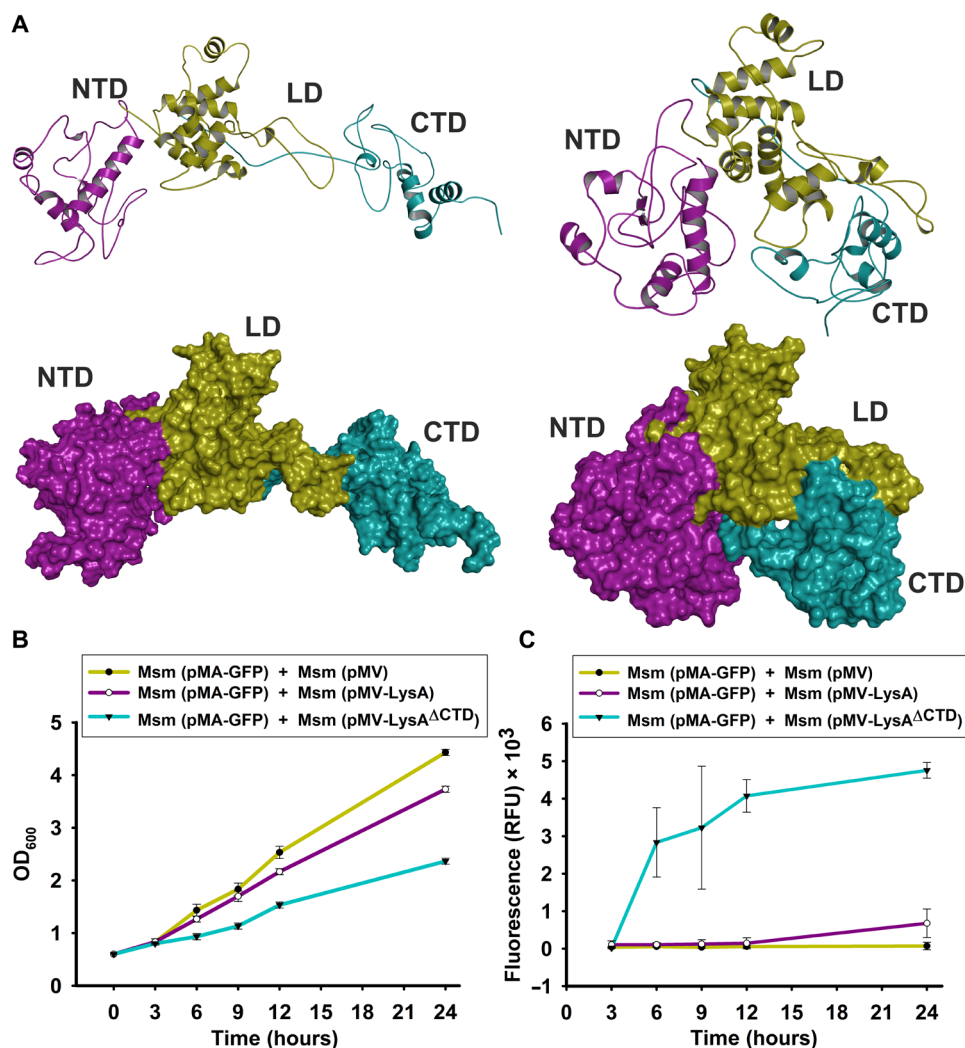
Fig. 5. Role of CTD in regulation of LysA mediated exogenous host cell lysis. (**A**) Visualizing MDS of the PG-induced open conformation of LysA after NAM-NAG-NAM removal (left). LysA regains its close conformation (right) once the substrate is removed from the complex, as shown in the final frame of 200-ns MDS. Space filled models for both are shown at the bottom of the panel. (**B**) Growth curve of mixed culture of Msm cells expressing either LysA or LysA$^{\Delta CTD}$ along with Msm cell expressing GFP after 0.2% acetamide induction. The data suggest reduction of growth only with culture expressing LysA$^{\Delta CTD}$, indicating exogenous cell lysis of the bystander cells (expressing only GFP). (**C**) GFP release in the growth curve samples [shown in (B)] was recorded in the supernatant collected at specified time points. The presence of GFP in the supernatant indicates lysis of bystander cell expressing GFP. In both (B) and (C), the data represent an average of measurements performed in triplicate; the error bars denote SD.

which results in the release of free LysA or LysA$^{\Delta CTD}$ protein into the medium (fig. S17B). Thus, this experimental setup allowed us to analyze whether these free proteins have any exogenous effect on bystander cells. As seen with our data (Fig. 5B and fig. S17A), the producer cells expressing full-length LysA do not have any substantial effect on the bystander population, which is reflected by the sustainable growth profile of the culture. However, the producer cell expressing LysA$^{\Delta CTD}$ has a substantial exogenous effect on bystanders, which is reflected by a notable decline in the growth of the bacterium. To further validate exogenous effect on bystander cells, we monitored GFP in the culture supernatant, which is released as a result of lysis of the bystander cells expressing GFP (Fig. 5C). Our fluorescence data show the presence of substantial amount of GFP in the culture having producer cell expressing LysA$^{\Delta CTD}$. On the other hand, no considerable GFP release is observed in the case of WT LysA, suggesting that LysA

uses some inhibitory mechanism that inhibits any exogenous effect on the bystander cells, which is absent in the case of LysA$^{\Delta CTD}$. When we put together this with our MDS data, it suggests that LysA reverses to the inactive conformation in the absence of substrate, which helps it to avoid any exogenous effect on the bystander cells. However, LysA$^{\Delta CTD}$ lacks this regulatory mechanism (because of the absence of CTD) and, therefore, remains in the active state and has an exogenous negative effect on bystander cells. The reduction in the population of uninfected nearby host cells is detrimental to phage propagation and survival. Thus, such inhibition of the exogenous activity of LysA is critical for phage fitness.

CTD of LysA inhibits premature host cell lysis

To further explore the significance of CTD of LysA in D29 physiology, we deleted the CTD-coding region from LysA gene in the

WT D29 phage (D29^{WT}) using the CRISPY-BRED method (fig. S18) (35) and generated D29$^{\Delta CTD}$ phage. We next monitored Msm growth after infecting it with different multiplicity of infection (MOI) of either D29^{WT} or D29$^{\Delta CTD}$. At MOI = 1, mycobacterial culture infected with D29$^{\Delta CTD}$ showed a steep decline in optical density at 600 nm (OD$_{600}$) within an hour of infection as compared to cells infected with D29^{WT} (Fig. 6A), suggesting rapid host cell lysis by D29$^{\Delta CTD}$ phage. Unexpectedly, at MOI = 0.1, we observed a slow decline in OD$_{600}$ when the bacteria were infected with D29$^{\Delta CTD}$ as compared to D29^{WT} (Fig. 6B), indicating reduced lytic efficiency of D29$^{\Delta CTD}$ in successive generations. Msm

cell lysis in both experiments was additionally confirmed by cell viability assay. These observations tempted us to investigate further the growth profile of these phages during the lytic cycle by carrying out one-step growth curve for both phages at MOI = 1. Our data revealed a 30-min reduction in the D29$^{\Delta CTD}$ latent period as compared to the D29^{WT} (Fig. 6C), suggesting a rapid onset of lysis due to the deletion of CTD. Not unexpected, therefore, that such rapid onset of host cell lysis led to a drastic reduction in both the burst size as estimated from our single-cell experiments (table S1) and the plaque size for the D29$^{\Delta CTD}$ as compared to D29^{WT} (Fig. 6D).
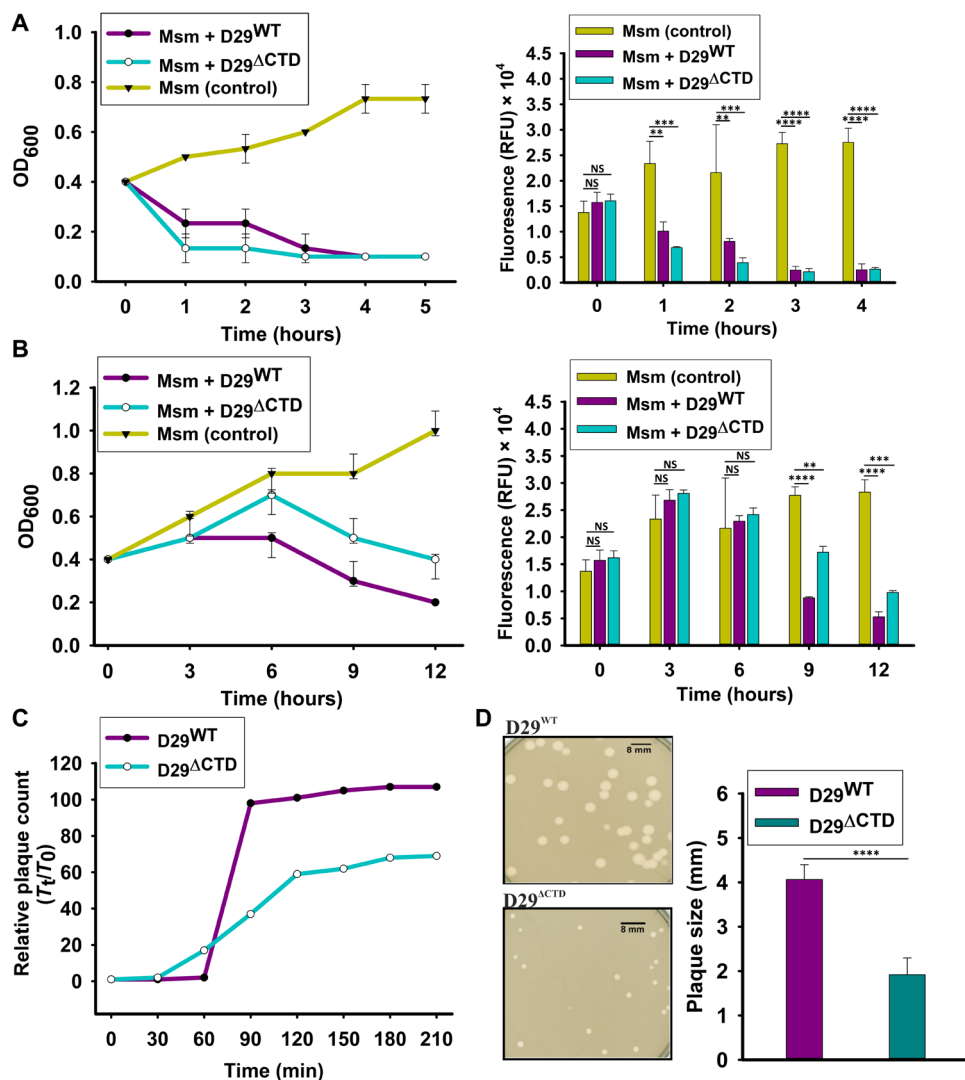
Fig. 6. Role of C-terminal domain of LysA in D29 phage mediated host cell lysis. The growth of Msm infected with D29^{WT} and D29$^{\Delta CTD}$ phages with MOI = 1 (**A**) and MOI = 0.1 (**B**) was compared to monitor the lytic efficiency of respective phages (left). The uninfected culture was used as a control in both experiments. Time 0 hours represents the time of addition of phages in the culture. The proportion of viable cells was measured at every time point by Alamar blue assay (right). The data at each time point represent an average of measurements performed in triplicate; the error bars denote SD. P value analysis: **$P < 0.001$; ***$P < 0.0005$; ****$P < 0.0001$; NS, not significant. (**C**) One-step growth curve with D29^{WT} and D29$^{\Delta CTD}$ phages was carried out to assess the impact of CTD deletion on different phases of phage replication cycle. Relative plaque count represents the free phages in the media after phage infection. It is measured by dividing plaque count at a particular time point (T_t) with plaque count at 0 hour (T_0). (**D**) Shown on the left is the one representative agar plate image of D29^{WT} and D29$^{\Delta CTD}$ phages infecting Msm cells. ImageJ software was used to measure the plaque diameter of both D29^{WT} and D29$^{\Delta CTD}$ phages, which is represented as plaque size (right). Plate diameter was set as a reference scale for measuring plaque diameter. The data represent an average of measurements performed in triplicate; the error bars denote the SD. P value analysis: ****$P < 0.0001$.

Our data thus clearly show that phage lacking CTD triggers rapid onset of host cell lysis, causing the reduction in burst size as compared to the WT. This reduced burst size is the reason for the slow decline in host population observed in case of D29$^{\Delta CTD}$ phage infection at lower MOI. Together with all the data presented here, we conclude that CTD inhibits LysA-mediated premature host cell lysis by keeping LysA in an inactive state, allowing the phage progeny to assemble in the cell. Host cell lysis after assembly of phage progeny will release an ample amount of progeny, which can infect other host cells, thus maximizing phage propagation.

Exploring the ability of purified LysA$^{\Delta CTD}$ protein to exogenously target mycobacterial cells

The mycolic acid–arabinogalactan layer present outside mycobacterial PG substantially affects the exogenous permeability of lysin proteins, but it does not completely bar their exogenous access. Substantial reduction in neighboring mycobacterial cells due to the exogenous activity of expressed LysA$^{\Delta CTD}$ protein encouraged us to explore the ability of purified LysA$^{\Delta CTD}$ protein to externally target mycobacterial cells. We, therefore, cloned, expressed, and purified LysA$^{\Delta CTD}$ and compared it with full-length LysA in terms of its activity and stability. LysA$^{\Delta CTD}$ showed more than 10-fold higher yield than the WT LysA (Fig. 7A); however, the reasons for this are currently unknown and have not been explored here. Furthermore, our zymography assay showed nearly equal enzymatic activity for both the proteins (Fig. 7B). Far-UV CD of LysA$^{\Delta CTD}$ indicates α-helical profile similar to LysA (Fig. 7C).

Cell wall of a bacterium plays a key role in maintaining its cellular integrity. Hence, an ability to hydrolyze mycobacterial PG is critical for targeting mycobacterial cells externally, which ultimately will lead to cell lysis. Upon being subjected to in vitro hydrolytic activity with FITC labeled Msm PG, LysA$^{\Delta CTD}$ protein showed higher activity than LysA and lysozyme protein. LysA$^{\Delta CTD}$ protein showed more than twofold higher activity than lysozyme (Fig. 7D). Similarly, LysA$^{\Delta CTD}$ showed promising results in turbidity reduction assay with Msm cells. The reduction in turbidity of the mycobacterial sample is an indicator of cell lysis. External treatment of LysA$^{\Delta CTD}$ protein shows a sharp reduction in turbidity within 30 min in comparison to LysA, suggesting rapid and efficient mycobacterial cell lysis (Fig. 7E).

Stability of lytic enzymes and retention of the ability to target bacterial cells after prolonged storage are critical factors in developing these enzymes as therapeutic candidates in future. In line with this thinking, LysA$^{\Delta CTD}$ stability and ability to lyse mycobacterial cells were checked after prolonged storage at 4°C. Turbidity reduction assay with stored LysA$^{\Delta CTD}$ protein shows substantial retention of lytic activity toward Msm cells in comparison with stored LysA protein (Fig. 7F).

Together, our data suggest that enzymatic efficiency of LysA$^{\Delta CTD}$ protein is much higher than LysA and other traditional cell wall–targeting enzymes like lysozyme. LysA$^{\Delta CTD}$ shows promising results in targeting mycobacterial cells externally. The high yield, stability, and ability of LysA$^{\Delta CTD}$ protein to retain enzymatic properties after prolonged storage make it an ideal phage enzyme-based candidate to externally target mycobacterial cells. However, this enzyme needs to be tested for its efficacy on pathogenic mycobacterial strains as well as other clinical aspects to develop it as a commercial therapeutic candidate against mycobacterial infections.

DISCUSSION

Host cell lysis during D29 mycobacteriophage lytic cycle is crucial for the release of viable progenies into the environment to infect new hosts. Any fluctuation in the host cell lysis, therefore, will have detrimental effect on phage proliferation. Thus, a precise regulation of lytic cycle is essential for maintaining a sustainable phage population. Mycobacterial PG layer poses itself as the biggest barrier in successful completion of D29 phage lytic cycle. To overcome this, D29 phage encodes LysA that targets mycobacterial PG. Here, we show that LysA, besides being critical for host cell lysis, also orchestrates various aspects of D29 life cycle. Thus, regulation of LysA is highly essential for phage physiology.

Here, we demonstrate that LysA exploits its modular nature to provide structural and functional plasticity required for lytic cycle regulation. Our data show that LysA exhibits two functional states—open and close conformations, which are structurally distinct from each other. Binding of PG to the cell wall binding domain (CTD) of LysA triggers the switch from close to open conformation, allowing the protein to become active. The arginines present in the CTD allow it to bind PG and are required for the establishment of a stable interaction between PG and CTD. Conceivably, PG with long chain of NAG and NAM requires a global arginine-rich cell wall binding domain in endolysins showing sequence similarity with LysA (36). Similar PG-induced conformation changes were also seen with PG turnover by lytic transglycosylase Slt of *Pseudomonas aeruginosa* (37). However, LysA harboring inactive CTD or LysA in the presence of noncanonical host substrate failed to elucidate similar conformational switch, which strongly suggests it to be CTD-mediated host-specific regulation.

LysA$^{\Delta CTD}$ being in active state, and mimicking a permanent open conformation, upon mild expression in Msm cells shows acute polar localization and demonstrates rapid host cell lysis. In contrast, LysA, due to its regulation by CTD, displays mild polar localization with notable cytoplasmic presence leading to comparatively slower host cell lysis (Fig. 8). The slow release of LysA protein in the supernatant compared to LysA$^{\Delta CTD}$ is an indicator of slow host cell lysis. Further, the inability of LysA to undergo conformational switch by itself in the absence of host substrate suggests that LysA is secreted in an inactive close conformation and that the host substrate–induced conformational switch upon translocation to the target site results in its activation and host cell lysis (Fig. 8). However, the exact mechanism of D29 LysA translocation to the periplasmic space is still not clear. Endolysins harboring signal peptides or signal-anchor release sequences use host secretory system for translocation to periplasm (38–42). Previously, we have shown that LysA expression in Msm cells leads to cell lysis, and the deletion of Holin from the D29 phage genome results in viable phage progeny after lytic cycle (23, 24, 43). However, a decrease in efficiency of phage-mediated host cell lysis due to the deletion of Holin was observed (43), which indicates a significance of Holin in LysA translocation during lytic cycle. Thus, we believe that despite the ability of LysA to translocate and lyse host cell independently of Holin in high-expression state, in the D29 phage, a Holin-mediated translocation of LysA is preferred for efficient host cell lysis during phage infection. Holin plays a crucial role in regulating the timing of host lysis, thereby acting as a "molecular clock." We postulate that the reason behind this preference is to avoid PG repairing by the host, which will otherwise nullify the endolysin effect. The PG repairing is prevented when endolysin is secreted after disruption of proton motive force (PMF) by Holin. The disruption of PMF is highly detrimental
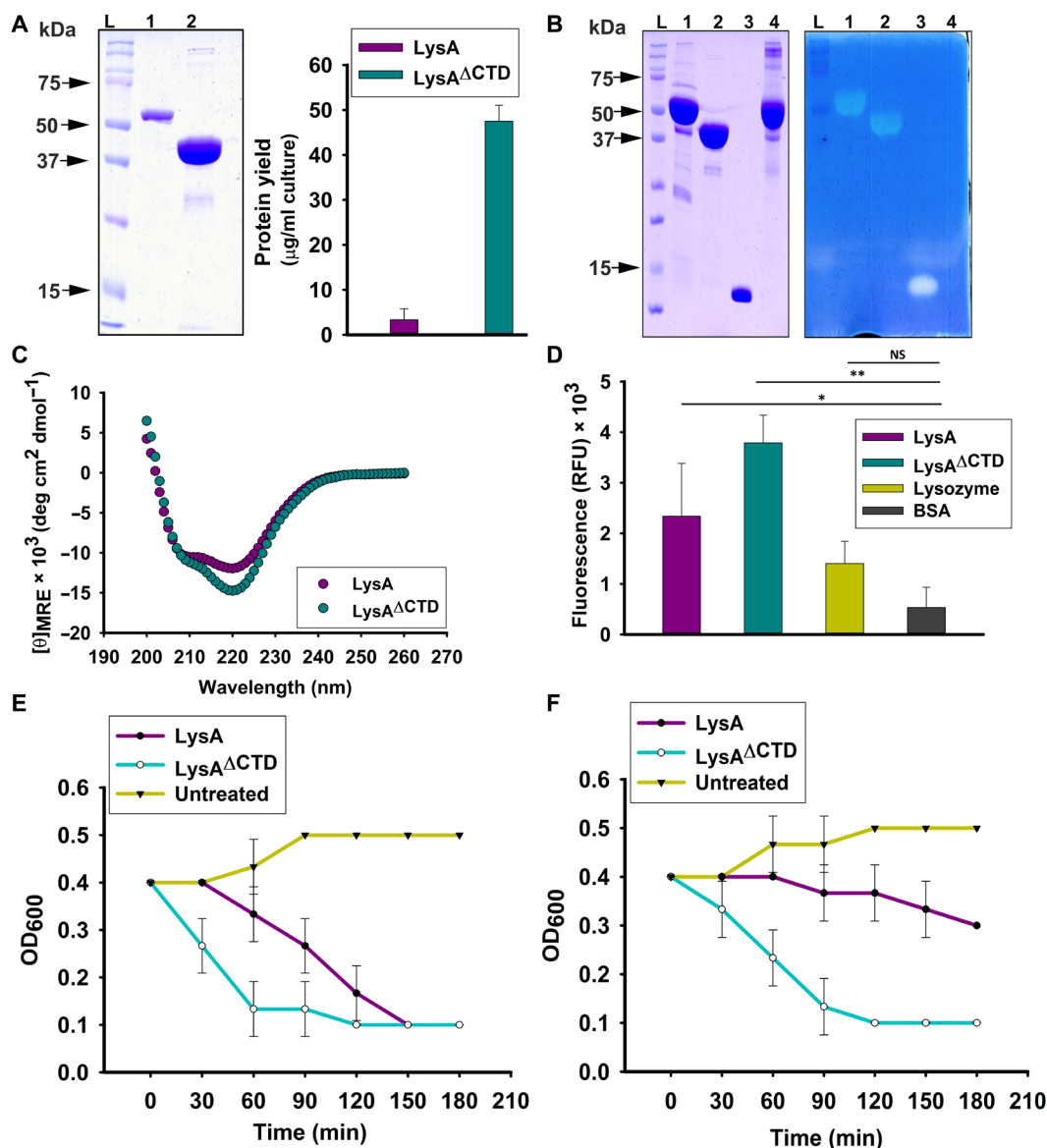
Fig. 7. Structural characterization of LysA△CTD and exploring its therapeutic potential. (**A**) LysA△CTD purification. Left panel shows Coomassie-stained SDS–polyacrylamide gel electrophoresis gel of purified LysA (lane 1) and LysA△CTD (lane 2). Right panel shows protein yield in micrograms per milliliter of culture upon expression from IPTG-inducible promoter in *E. coli* BL21(DE3). LysA△CTD shows more than 10-fold higher yield than WT LysA. (**B**) Analysis of PG hydrolytic activity of proteins using Zymography assay. Left panel shows loading control of proteins used in zymography assay. Right panel shows zymography gel. In both panels, lanes 1, 2, 3, and 4 represent LysA, LysA△CTD, lysozyme (positive control), and BSA (negative control), respectively. L represents molecular weight marker with few bands marked. LysA△CTD and LysA display similar level of PG hydrolytic activity. (**C**) Representative far-UV CD spectra of purified LysA and LysA△CTD are shown as mean residue ellipticity. Both proteins show largely α-helical profile. An average of three measurements in each case is presented here. (**D**) In vitro PG hydrolysis activity with FITC-labeled Msm PG. Samples treated with different proteins were excited at 495 nm, and emission was recorded at 520 nm. LysA△CTD shows substantially higher activity (as high fluorescence) than other proteins. Data at each time point represent an average of measurements performed in triplicate; the error bars denote SD. *P* value: *$P < 0.05$; **$P < 0.001$; NS, not significant. (**E**) Turbidity reduction assay with Msm cells when treated with different proteins. Untreated cells were used as control in the experiment. (**F**) Turbidity reduction assay with stored proteins (~1 year at 4°C). Data suggest that LysA△CTD retains its lytic activity, whereas LysA loses its activity after prolonged storage. The data at each time point represent an average of measurements performed in triplicate; the error bars denote the SD.

for the host and will engage the host response system completely off from PG repairing toward tackling the imbalance due to disrupted PMF. LysA accumulates near polar region of inner membrane as seen in our microscopy data (Fig. 4D) and, upon disruption of PMF, translocates to the periplasmic space to target host PG, which ultimately leads to efficient host cell lysis. While the arginine abundance in CTD

of LysA facilitates stable interaction with host PG, we believe that it may also have a function in localizing the protein at the negatively charged cell membrane (Fig. 4D), thus delaying passage through the membrane (which is no longer the case for LysA△CTD, due to the absence of CTD). However, in the D29 phage, Holin-dependent translocation of LysA is not obligatory, as seen in this and in our previous
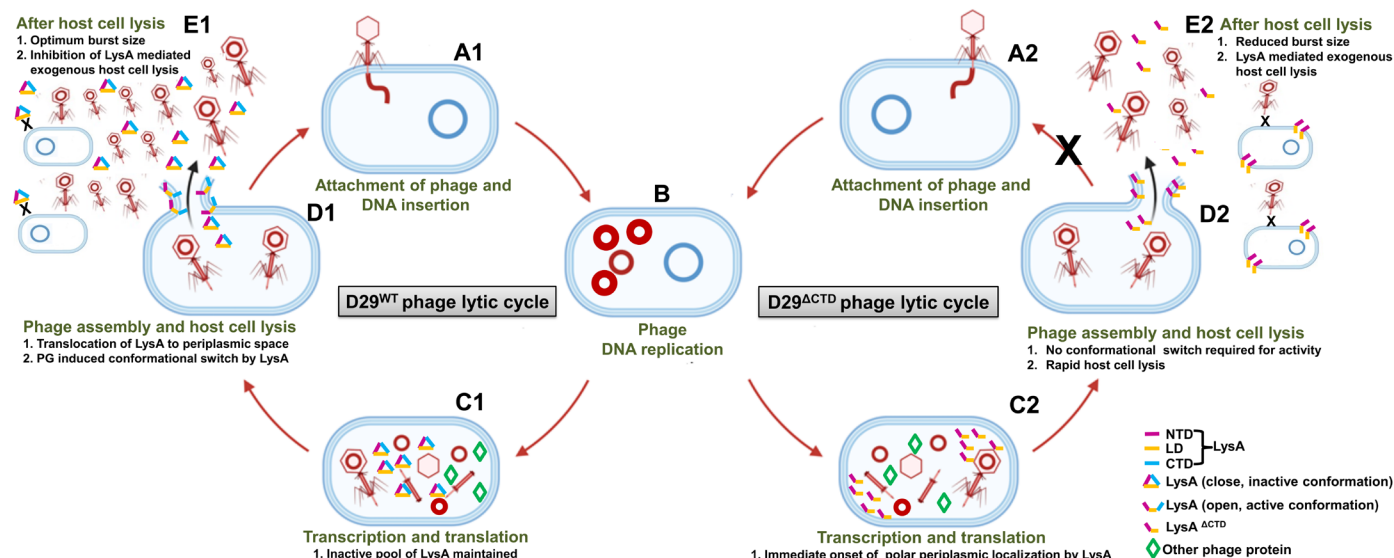
Fig. 8. Schematic showing the significance of CTD-mediated LysA regulation at various stages of D29 life cycle. Left panel shows LysA-mediated regulation of D29 lytic cycle; right panel displays the effect of CTD deletion on the same. Onset of lytic cycle occurs by phage attachment (**A1** and **A2**) on host cell surface, followed by insertion of phage DNA. (**B**) Phage DNA replication inside host cell, followed by transcription and translation of phage genes to synthesize phage proteins required for production of phage progeny. To release newly assembled virions, phages encode LysA or LysA$^{\Delta CTD}$, which targets host PG. (**C1**) LysA is secreted in an inactive state (close conformation), accumulating inside the host cytoplasm and slowly localizing to periplasmic space to target host PG layer. (**C2**) LysA$^{\Delta CTD}$ is secreted as open active form due to disruption of close conformation caused by CTD deletion; this leads to rapid polar periplasmic localization of protein with no cytoplasmic accumulation. (**D1**) Recognition of host PG by CTD induces conformational switch in LysA from inactive close to active open conformation, allowing catalytic domains to access host PG, ultimately causing host cell lysis. However, CTD-mediated structural regulation of LysA inhibits rapid host cell lysis. (**D2**) Because LysA$^{\Delta CTD}$ is already active, it induces rapid host cell lysis. (**E1**) Moderate pace of host cell lysis due to LysA structural regulation allows phage to exploit host carrying capacity and achieve maximum burst size. Ability of LysA to regain inactive conformation after host lysis inhibits exogenous targeting of neighboring uninfected cells, which is essential for phage propagation in successive generation. (**E2**) Rapid host cell lysis due to lack of structural regulation in LysA causes drastic reduction in burst size. Inability of LysA$^{\Delta CTD}$ to achieve inactive conformation after host lysis causes exogenous targeting of neighboring uninfected cells, thus effecting phage propagation in successive generation.

studies. LysA can translocate to the target site without Holin; however, in the natural scenario of phage infection, Holin-mediated translocation may be preferred for physiological benefits over the host response system.

D29$^{\Delta CTD}$ phage lacking inactive-active state regulation of LysA demonstrated reduced latent period and a rapid onset of host cell lysis, thus resulting in a consequential decrease in the burst size, ultimately causing reduced MOI in successive generations. Thus, to maintain a stable phage population, it is important to attain an optimum burst size, which is possible by avoiding premature host cell lysis through a tightly regulated and well-timed host cell lysis mechanism during the lytic cycle. Hence, in a rapidly changing host environment, CTD-mediated structural and functional regulation of LysA plays a pivotal physiological role in phage propagation and fitness by facilitating maximum utilization of host carrying capacity (Fig. 8).

Gram-negative bacteria outer membrane acts as a barrier against any exogenous activity of lytic enzymes released into the environment after host lysis. On the other hand, in Gram-positive bacteria, the uninfected bystanders are susceptible to exogenous lysis by the released endolysin (*44*). Our data suggest that the close inactive conformation adopted by LysA in absence of host PG inhibits the deleterious effect on neighboring uninfected host cells as seen in LysA$^{\Delta CTD}$ due to the disruption of conformational switch (Fig. 8). The diffusion of endolysin molecules will be rapid as compared to phage particle in the environment, and, therefore, CTD-mediated conformational regulation of LysA becomes important in maintaining host-phage population

dynamics by ensuring host availability for progenies of successive generations.

MATERIALS AND METHODS
Bacterial strains and growth conditions
Cloning experiments and protein expression were carried out using XL1-Blue (Stratagene) and BL21 (DE3) (Novagen) strains of *E. coli*, respectively. Luria-Bertani (LB) medium (Difco) was used to culture bacteria supplemented with ampicillin (100 µg ml^{-1}) at 37°C with constant shaking at 200 rpm unless specified otherwise. Middlebrook 7H9 medium (Difco) supplemented with 2% glucose, 10% OADC (Oleic acid, Albumin, Dextrose, Catalase; Difco), and 0.05% Tween 80 was used to culture Msm along with kanamycin (50 µg ml^{-1}). Agar (1.5%) was used for solid medium culture, while 0.75% agar was used for the phage experiment.

Construction of recombinant plasmids
The recombinant plasmid used in this study and the oligos used to generate them are listed in tables S2 and S3, respectively. pMA-GFP vector was used to carry out expression studies with Msm (*29*). *gp10* gene (coding for LysA) was amplified with NTD_For and GP10_Rev primers using D29 genomic DNA as a template. Similarly, NTD_For and GP10_LD_Rev primers were used to amplify LysA$^{\Delta CTD}$-coding gene. We have used two versions of GFP-tagged LysA and LysA$^{\Delta CTD}$. One version has the GFP at the N terminus of the protein, and the other

version has the GFP present at the C terminus. To achieve this, both *gp10* and *gp10ΔCTD* genes were cloned at the Hpa I site for N-terminal GFP tagging, and at the Eco RV site for C-terminal GFP tagging. All the recombinant plasmids and mutations generated were confirmed by DNA sequencing.

Protein expression and purification

Plasmids pET-GP10, pET-GP10ΔCTD, pET-GFP, pET-GP10CTD, and pET-CTDGFP, as listed in table S2, were used to express and purify LysA, LysA ΔCTD, GFP, CTD, and CTD tagged with a GFP (CTD-GFP), respectively, as described previously (*23*, *25*). All the cysteine and arginine mutations in LysA and CTD were carried out with the same expression system, i.e., pET-GP10, pET-GP10CTD, and pET-GP10CTDGFP for protein purification. *E. coli* BL21(DE3) harboring respective recombinant plasmids in the pET expression system were cultured at 37°C with constant shaking at 200 rpm. The cells were induced with 0.3 mM isopropyl-β-D-thiogalactopyranoside upon reaching OD_{600} ~0.6 and then further allowed to grow at 22°C for 8 hours with constant shaking at 150 rpm. Cells were then harvested and resuspended in lysis buffer [40 mM tris-Cl (pH 8.0), 400 mM NaCl, and 5 mM 2-mercaptoethanol]. The resuspended cell was lyzed by sonication. The supernatant obtained after harvesting lysate was incubated with pre-equilibrated nickel–nitrilotriacetic acid (Qiagen) beads for 2 hours. Beads were washed with wash buffer containing 40 mM tris-Cl (pH 8.0), 500 mM NaCl, 25 mM imidazole, and 5 mM 2-mercaptoethanol. Elution of proteins was carried out in the elution buffer containing 40 mM tris-Cl (pH 8.0), 400 mM NaCl, 300 mM imidazole, and 5 mM 2-mercaptoethanol. Elution fractions were dialyzed against the storage buffer containing 40 mM tris-Cl (pH 8.0), 200 mM NaCl, and 1 mM dithiothreitol (DTT) at 4°C for experiments. The dialysis buffer for protein used for FRET experiments was devoid of DTT.

PG preparation

PG was extracted from Msm cells using method as described elsewhere with some modifications (*23*, *45*). Cells were grown in 2 liters of Middlebrook 7H9 medium (Difco) supplemented with 2% glucose, and 0.05% Tween 80 until the late log phase. Cells were then harvested and resuspended in 100 ml of breaking buffer [20 mm tris-Cl (pH 8.0), 500 mM NaCl, and 10% glycerol]. Resuspended cells were subjected to a cell homogenizer (Constant Systems Ltd.) at 206.8 MPa. The homogenized suspension was further sonicated for 10 min (a pulse duration of 15 s on and 15 s off) for complete lysis. The lysate was further centrifuged (18,000 rpm for 30 min at room temperature), and the pellet was resuspended in the breaking buffer having 2% SDS and incubated for 3 hours at 45°C. The sample was allowed to cool down, followed by centrifugation at 18,000 rpm for 30 min at room temperature. The pellet was resuspended in 1% SDS along with protease by *Streptomyces griseus* (100 μg/ml final concentration). The resuspended sample was stirred slowly at 45°C for 3 hours and then at 80°C for 1 hour. The suspension was then allowed to cool down and centrifuged at 18,000 rpm for 30 min. The resulting pellet was resuspended in 1% SDS and sonicated in the water bath. The resuspension was washed with deionized water multiple times to remove SDS completely. The resulting mycolic acid arabinogalactan PG was extracted using ethanol–diethyl ether (1:1) and dried. The sample was then treated with 0.5% KOH in methanol and stirred at 37°C for 48 hours to hydrolyze mycolic acid. The sample was then centrifuged, and the pellet was washed with methanol and diethyl ether multiple times and

dried under vacuum. The sample was then subjected to treatment with 0.05 N H_2SO_4 at 37°C and incubated for 3 days to get rid of arabinogalactan. The sample, which is insoluble, was washed four times with deionized water, dried under vacuum, and stored at −80°C.

E. coli PG was extracted from cells by following the method as described previously with some modifications (*46*). Cells were grown in LB media until the midexponential phase, harvested, and resuspended in 100 mM NaCl. The resuspended cells were added drop by drop to preheated (80°C in a water bath) 12-ml 4% (w/v) SDS with constant stirring. An additional 12 ml of hot 8% SDS was added to it, and the sample was incubated at 80°C for 1 hour. The sample was washed multiple times with deionized water to get rid of SDS and then treated with deoxyribonuclease I and ribonuclease. The sample was then digested overnight with trypsin. The sample was denatured with 4% SDS at 80°C and washed multiple times with deionized water to get rid of SDS. The resulting *E. coli* PG was extracted using ethanol–diethyl ether (1:1), vacuum-dried, and stored at −80°C.

PG binding assay

The protein binding to mycobacterial PG was examined as described previously (*23*, *47*), with some modifications. Briefly, Msm PG stock (5 mg/ml) was prepared in a binding buffer [25 mM tris-Cl (pH 8.0), 200 mM NaCl, and 0.05% Triton X-100]. Peptidoglycan (500 μl) sample was incubated with 5 μM of desired protein of interest at 37°C for 2 hours with constant mixing. The mixture was then centrifuged at 13,000 rpm for 10 min, and the pellet was subjected to two rounds of washing with 500 μl of binding buffer. The washed pellet was resuspended in 50 μl of 8 M urea and centrifuged at 13,000 rpm for 10 min. The supernatant was subjected to SDS–polyacrylamide gel electrophoresis (SDS-PAGE); in this experiment, the presence of a protein band in the respective sample would confirm its PG binding activity.

Bacterial cell binding assay

The cell binding assay was carried out essentially as described previously (*25*). Briefly, Msm culture was grown until OD_{600} ~0.6 and normalized with respect to the experimental setup. Cells in the sample were harvested by centrifugation at 8000 rpm, resuspended in binding buffer [25 mM tris-Cl (pH 8.0), 200 mM NaCl, and 1% Triton X-100], and incubated at 37°C for 2 hours with constant shaking. Cells were then harvested, resuspended in a binding buffer with 0.05% Triton X-100, and incubated with 10 μM GFP-tagged protein at 37°C for 2 hours. This mixture was then centrifuged, and the pellet was washed twice with the binding buffer to eliminate any unbound protein. GFP fluorescence of the sample was then recorded on SpectraMax M5 multimode reader (Molecular Devices) by keeping the excitation and the emission wavelengths as 488 and 509 nm, respectively.

Labeling of protein with fluorophore

Site-directed mutagenesis (SDM) was carried out essentially as described previously (*48–50*), using a pair of primers, and the mutations were confirmed by DNA sequencing. SDM was performed to introduce cysteine pairs, with one cysteine in the NTD and the other in the CTD of LysA. The purified proteins were labeled with thiol-reactive probes, 1,5-IAEDANS and 6-IAF essentially as described previously (*27*, *28*). Briefly, proteins harboring cysteine pairs were subjected to dialysis against the labeling buffer [40 mM tris-Cl (pH 8.0), 200 mM NaCl, and 5% glycerol]. Protein concentration was determined by recording its absorbance at 280 nm, and using its molar extinction

coefficient value as 101,300 M^{-1} cm^{-1} as derived from the protein sequence using the protparam tool available at ExPasy (https://web.expasy.org/protparam/). Ten-fold molar excess of tris(2-carboxyethyl) phosphine was added, and the protein sample was incubated at 4°C for 30 minutes to reduce all the disulfides. Later, IAF was added in the molar ratio of 1:4 for single Cys-containing proteins and 1:1 (protein:IAF) ratio for two-Cys–containing proteins. The samples were incubated at 4°C for 12 hours in the dark. IAF-labeled protein was further labeled with IAEDANS following similar method, but with a molar ratio of 1:4 (IAEDANS: Protein). The labeling reaction was quenched by an addition of 10 mM final concentration of DTT. Excess free dye and DTT were removed using a PD10 spin column (Cytiva) packed with Sephadex G-25 matrix, following the manufacturer's instructions. Similarly, proteins were also labeled with IAF and QSY-9 C5-maleimide (Thermo Fisher Scientific). The Dye:protein ratio was calculated by recording the absorbance of the samples at 280, 336, and 492 nm, and using the formula

$$\text{Moles of dye per mole of protein} = (A_{\lambda\text{max}} \text{ of the labeled protein}/\varepsilon' \times M)$$

where ε' is molar extinction coefficient of the fluorescent dye and M is protein concentration, which was calculated as

$$\text{Protein concentration } (M) = [A_{280} - (A_{\lambda\text{max}} \times \text{ Correction factor})/\varepsilon]$$

where ε is the protein molar extinction coefficient; $A_{\lambda\text{max}}$ is the absorbance (A) of a dye solution measured at the wavelength maximum (λ_{max}) for the dye molecule; and CF is the correction factor, adjusted for the dye contribution at 280 nm.

Förster resonance energy transfer
FRET experiments were carried out with the fluorophore-labeled proteins (27, 28). Protein at a final concentration of ~10 µM was used for the fluorescence measurements on FluoroMax 4C spectrofluorimeter (Horiba). The samples were excited with donor excitation wavelength, and the emission spectra were recorded in the range of both donor and acceptor. Samples labeled with 1,5-IAEDANS (donor) and 6-IAF (acceptor) FRET pair were excited at 336 nm, and the emission was recorded from 360 to 600 nm, whereas samples labeled with 6-IAF (donor) and quencher QSY-9 (acceptor) were excited at 494 nm, and the emission was recorded from 500 to 600 nm. Mono-labeled protein samples were used as control. The fluorescence spectral data were subjected to minimal two-dimensional smoothing using SigmaPlot 12.5. However, smoothening did not affect interpretation of data in any manner.

Growth curve and cell viability assay
Effect of protein expression on the growth of Msm was monitored in terms of optical density of the culture at 600 nm (OD_{600}). Briefly, protein expression in Msm was carried out using the pMV-acetamide vector expression system (23, 24). The bacterium harboring the plasmid was grown in MB7H9 broth at 37°C with constant shaking at 200 rpm. At OD_{600} ~0.6, the culture was induced with 0.2% acetamide and the bacterial growth was monitored by measuring OD_{600} every 3 hours. Cell viability assay was carried out essentially as described previously (24). Briefly, 10% (v/v) alamarBlue reagent (Thermo Fisher Scientific) was added to the bacterial samples collected from the

induced culture every 3 hours and incubated at 37°C for 1 hour. Fluorescence of the samples was then measured on SpectraMax M5 multimode reader by using the excitation and emission wavelengths as 540 and 590 nm, respectively.

Western blotting
Western blotting assay was carried out essentially as described previously (23). Anti-gp10 antibodies were used as primary antibodies for probing LysA protein and its variant. Goat anti-Rabbit IgG (H+L) Secondary Antibody, DyLight 800 (catalog no. SA5-35571; Invitrogen) was used as secondary antibody. The blot was imaged on LI-COR image scanner.

GFP release assay
Msm cells expressing GFP or protein tagged with GFP were harvested at specific time points of growth curve by centrifugation at 8000 rpm at 4°C for 5 min. Fluorescence of collected 200 µl of supernatant was then measured on SpectraMax M5 multimode reader by using the excitation and emission wavelengths as 488 and 509 nm, respectively.

Cell wall modification assays
Phenotypic assessment of alteration in the cell wall of Msm was carried out by monitoring sliding motility, colony morphology, and Congo red dye retention agar assay, essentially as described previously (51, 52). Briefly, Msm cells carrying pMA vector expressing gene of interest were grown in MB7H9 (Difco) supplemented with 2% glucose, 0.05% Tween 80, and kanamycin (50 µg ml^{-1}). At OD_{600} ~0.6, the culture was induced with 0.1% acetamide. Two microliters of the culture 3 hours after induction were spotted for all the assays.

Fluorescence microscopy imaging
Msm cells expressing pMA-GFP vector harboring LysA and $LysA^{\Delta CTD}$, were imaged essentially as described previously (53), on Olympus Confocal Laser Scanning Microscope–FV3000 under a 100× oil-immersion objective. Briefly, cells were induced with 0.1% acetamide at 37°C for 1 hour with constant shaking to express the cloned gene. Induced culture (200 µl) was counterstained with FM4-64 dye as per manufacturer's instructions. Samples were then washed with PBST (phosphate-buffered saline with Tween 20) thrice and resuspended in 200 µl of PBST. Sample (2 µl) was spotted on a 1% agarose pad, placed on a microscope slide, and sealed. Images were captured using GFP (488 nm) and FM4-64 (506 nm) filters and processed using ImageJ and Adobe Photoshop.

Msm growth curve during phage infection
Phage-mediated lysis of Msm was examined essentially as described previously (24, 54). Briefly, cells were grown in MB7H9 culture medium supplemented with 1 mM $CaCl_2$ and 10% OADC. Culture at OD_{600} ~0.6 was subjected to phage infection and incubated at 37°C for 6 hours with gentle shaking at 50 rpm. The experiments were carried out with MOI of 1 and 0.1. The OD_{600} of the culture was measured every hour and plotted.

One-step growth, burst size, and plaque size estimation
These experiments were carried out essentially as described previously (24, 54). For one-step growth experiment, exponentially growing Msm cells were resuspended in 1 ml of phage dilution buffer [10 mM tris-Cl (pH 7.5), 10 mM $MgSO_4$, and 68.5 mM NaCl] supplemented with 1 mM $CaCl_2$ with the infection being carried out at

MOI = 1. The suspension was incubated at 37°C for 20 min allowing phage adsorption. The samples were then treated with 100 μl of 0.4% H_2SO_4 (v/v) for 5 min to inactivate nonadsorbed phages. The inactivation was immediately followed by an addition of 100 μl of 0.4% NaOH to neutralize the acid. The samples were then diluted 1:100 in MB7H9 medium supplemented with 10% OADC and 1 mM $CaCl_2$. At every 30-min time interval, 1 ml of sample was withdrawn and serially diluted. The diluted sample (100 μl) was mixed with 200 μl of Msm culture and plated with MB7H9 medium as a top agar lawn. Plates were then incubated at 37°C for 12 hours, and resulting plaques were counted. The phage titer was determined for each sample and plotted with respect to time to analyze the growth profile. Burst size was measured by carrying out single-cell phage infection experiments. Briefly, the phage-infected samples were diluted to get 0.33 phage-infected mycobacterial cells ml^{-1} of broth. The diluted sample was distributed equally (1 ml per vial) and incubated for 2 hours at 37°C. The sample and 200 μl of Msm cells were plated on an MB7H9 agar plate along with MB7H9 soft agar supplemented with 1 mM $CaCl_2$. Plaques were observed after 12 hours of incubation at 37°C. Burst size was determined using Poisson distribution [BS: $P(x; \lambda) = (e - \lambda)(\lambda x)/x!$, where $P(x)$ is the probability of samples having x infected cells, λ is the average number of infected cells per tube and BS is the total plaque count in the 50 plates divided by the total number of infected cells]. For plaque size estimation, 200 μl of Msm cells was mixed with 100 μl of the sample obtained at the end of the saturation phase (210 min) of the one-step growth curve and plated with MB7H9 medium as a top agar lawn. Plaque size was measured after 12 hours of incubation at 37°C. Plaque diameter was measured using ImageJ software (v1.48t), where the standard petri dish diameter (90 mm) was kept as a reference scale.

Construction of mutants

SDM was carried out to generate all the mutants using transfer-PCR (polymerase chain reaction) (48, 55). PCR was carried out using mutagenic primers and plasmids harboring respective WT genes as templates. After PCR, the template DNA was removed by digestion using Dpn I and was further used to transform *E. coli* XL1-Blue (Stratagene). The mutation was further verified by Sanger sequencing. All the primers used for creating mutations are listed in table S3.

Construction of D29$^{\Delta CTD}$ phage

The D29$^{\Delta CTD}$ phage was prepared using the CRISPY-BRED method as described previously (35). A 506-bp-long allelic exchange substrate (AES) was prepared to introduce the desired deletion. The genomic DNA of D29 phage was used as a template in a PCR to prepare the DNA segment carrying the flanking regions of the desired deletion of CTD. The 268-bp-long region upstream of CTD was generated using CTD_up_For and CTD_up_Rev primers (table S3). Similarly, a 274-bp-long DNA segment downstream of CTD was amplified using CTD_down_For and CTD_down_Rev primers (table S3). Both PCR products were mixed together and subjected to overlapping PCR using CTD_up_For and CTD_down_Rev primers to generate AES with the desired deletion of the CTD region. The AES was coelectroporated with D29 phage genomic DNA in Msm cells carrying pJV53 plasmid (gift from G. Hatfull, University of Pittsburgh, USA; Addgene plasmid no. 26904) (56) modified to harbor hygromycin resistance gene. This modification will be presented separately elsewhere. After electroporation, the cells were recovered in MB7H9 medium

supplemented with 10% OADC (v/v) and 1 mM $CaCl_2$ for 4 hours at 37°C. The phages released after 4 hours of incubation were mixed with counterselection strain. This selection strain harbored a pCRISPR plasmid (pCRISPRx-Sth1Cas9-L5, a gift from W. Bitter; Addgene Plasmid no. 140993) (57) carrying guide RNA that targeted the CTD-coding region. It was then plated as a top agar lawn on MB7H9 media plate with kanamycin as selection marker and anhydrotetracycline to induce Cas9 expression from the CRISPR plasmid. Primary plaques were then picked and resuspended in phage dilution buffer [10 mM tris-Cl (pH 7.5), 10 mM $MgSO_4$, 68.5 mM NaCl, and 1 mM $CaCl_2$]. The obtained phages were PCR verified for CTD deletion followed by confirmation by DNA sequencing.

CD spectroscopic analysis of proteins

Secondary structure of proteins was assessed using far-UV CD spectroscopic measurements essentially as described previously (24, 58). Briefly, purified proteins were dialyzed against CD buffer [20 mM tris-HCl (pH 8.0), 50 mM NaCl, and 5 mM β-mercaptoethanol]. Proteins at a final concentration of 5 μM were used for CD analysis. Far-UV CD spectra of all the proteins were recorded at 25°C in a quartz cuvette with a path length of 1 mm, and averaged over three accumulations, subtracted from the buffer, smoothened using the means-movement method, and represented as either molar ellipticity or mean residue ellipticity.

PG hydrolysis assay

PG hydrolytic activity of the proteins was assessed in vitro by zymography (23, 24, 59), and by monitoring the hydrolysis of fluorescently-labeled PG. SDS-PAGE gels for zymography were prepared using 0.2% *Micrococcus lysodeikticus* cells (Sigma-Aldrich) as substrate. The experiment was carried out as described with some modifications. Briefly, 10 μM of protein boiled with SDS loading buffer was subjected to SDS-PAGE on a gel containing the substrate. After electrophoresis, the gel was washed twice with the renaturation buffer [25 mM tris-HCl, (pH 8.0), 1% Triton X-100, and 5 mM EDTA] and incubated in the same buffer at room temperature for 12 hours. It was then developed as described and imaged (23, 24). Bovine serum albumin and lysozyme were used as negative and positive controls, respectively. For in vitro PG hydrolysis assay, FITC-labeled Msm PG was prepared as described previously (60). Labeled PG was washed multiple times with a binding buffer [25 mM tris-Cl (pH 8.0), 200 mM NaCl, and 0.05% Triton X-100] to remove any unbound dye. To assess the hydrolytic activity, the FITC labeled Msm PG resuspended in a binding buffer was incubated with 10 μM of either LysA or LysA$^{\Delta CTD}$ proteins at 37°C for 1 hour. The fluorescence intensity of the collected supernatant was measured by exciting the sample at 492 nm and recording the emission at 515 nm on SpectraMax M5 multimode reader.

Statistical analysis

Statistical analyses such as unpaired two-tailed Student's t test and two-way analysis of variance (ANOVA) were performed using GraphPad Prism 7.0 (GraphPad Software Inc., San Diego, CA USA).

In silico protein structure prediction and refinement

LysA protein structure was predicted and refined using GalaxyWEB server (61), while CTD protein structure was predicted using QUARK ab-initio protein structure prediction server (62). Structural validation was done using the SAVESv6.0 server. The protein model with the best score was selected and subjected to 100-ns MDS using

GROMACS v2020.5 (*63*). The final structure obtained after MDS was used for all the structural analysis.

MDS studies

The input files for MDS of protein in the aqueous solvent environment were generated using the solution builder module of the CHARMM-GUI web server (*64*). The water box with an edge distance of 10 Å was used to hydrate protein, and 0.2 M NaCl was placed with the Monte Carlo method to neutralize the charges. The system contained a water box along with Na^+ and $Cl^−$ ions and a protein molecule embedded in it. A CHARMM-36 force field was used with NPT (constant particle number, pressure, and temperature) ensemble with no external surface tension to generate the input files. MDS was carried out for different time periods using GROMACS v2020.5 (*63*). Stepwise energy minimization and equilibration were carried out, and in the end, a production run with zero restraints was executed to generate the final trajectory. The trajectory analysis was carried out using GROMACS v2020.5 and visualized using PyMOL.

Supplementary Materials

This PDF file includes:
Figs. S1 to S18
Tables S1 to S3

REFERENCES AND NOTES

1. E. Harding, WHO global progress report on tuberculosis elimination. *Lancet Respir. Med.* **8**, 19 (2020).
2. S. Lakoh, G. A. Yendewa, Multidrug-resistant tuberculosis in Sierra Leone. *Lancet Glob. Health* **10**, e459–e460 (2022).
3. D. J. Payne, M. N. Gwynn, D. J. Holmes, D. L. Pompliano, Drugs for bad bugs: Confronting the challenges of antibacterial discovery. *Nat. Rev. Drug Discov.* **6**, 29–40 (2007).
4. Z. S. Bhat, M. A. Rather, M. Maqbool, H. U. L. Lah, S. K. Yousuf, Z. Ahmad, Cell wall: A versatile fountain of drug targets in *Mycobacterium tuberculosis*. *Biomed. Pharmacother* **95**, 1520–1534 (2017).
5. E. C. Hett, E. J. Rubin, Bacterial growth and cell division: A mycobacterial perspective. *Microbiol Mol Biol Rev.* **72**, 126–156 (2008).
6. A. Koul, E. Arnoult, N. Lounis, J. Guillemont, K. Andries, The challenge of new drug discovery for tuberculosis. *Nature* **469**, 483–490 (2011).
7. A. Maitra, T. Munshi, J. Healy, L. T. Martin, W. Vollmer, N. H. Keep, S. Bhakta, Cell wall peptidoglycan in *Mycobacterium tuberculosis*: An Achilles' heel for the TB-causing pathogen. *FEMS Microbiol. Rev.* **43**, 548–575 (2019).
8. L. J. Alderwick, G. Harrison, G. S. Lloyd, H. L. Birch, The Mycobacterial Cell Wall—Peptidoglycan and Arabinogalactan. *Cold Spring Harb. Perspect. Med.* **5**, a021113 (2015).
9. S. M. Batt, C. E. Burke, A. R. Moorey, G. S. Besra, Antibiotics and resistance: the two-sided coin of the mycobacterial cell wall. *Cell Surf* **6**, 100044 (2020).
10. F. Squeglia, A. Ruggiero, R. Berisio, Chemistry of peptidoglycan in *Mycobacterium tuberculosis* life cycle: An off-the-wall balance of synthesis and degradation. *Chemistry* **24**, 2533–2546 (2018).
11. J. E. Hugonnet, J. S. Blanchard, Irreversible inhibition of the *Mycobacterium tuberculosis* beta-lactamase by clavulanate. *Biochemistry* **46**, 11998–12004 (2007).
12. D. A. Harris, M. Ruger, M. A. Reagan, F. J. Wolf, R. L. Peck, H. Wallick, H. B. Woodruff, Discovery, development, and antimicrobial properties of D-4-amino-3-isoxazolidone (oxamycin), a new antibiotic produced by *Streptomyces garyphalus* n. sp. *Antibiot Chemother* **5**, 183–193 (1955).
13. K. Dheda, T. Gumbo, N. R. Gandhi, M. Murray, G. Theron, Z. Udwadia, G. B. Migliori, R. Warren, Global control of tuberculosis: from extensively drug-resistant to untreatable tuberculosis. *Lancet Respir. Med.* **2**, 321–338 (2014).
14. M. Klopper, R. M. Warren, C. Hayes, N. C. Gey van Pittius, E. M. Streicher, B. Müller, F. A. Sirgel, M. Chabula-Nxiweni, E. Hoosain, G. Coetzee, P. David van Helden, T. C. Victor, A. P. Trollip, Emergence and spread of extensively and totally drug-resistant Tuberculosis, South Africa. *Emerg. Infect. Dis.* **19**, 449–455 (2013).
15. F. Coll, J. Phelan, G. A. Hill-Cawthorne, M. B. Nair, K. Mallard, S. Ali, A. M. Abdallah, S. Alghamdi, M. Alsomali, A. O. Ahmed, S. Portelli, Y. Oppong, A. Alves, T. B. Bessa, S. Campino, M. Caws, A. Chatterjee, A. C. Crampin, K. Dheda, N. Furnham, J. R. Glynn,

L. Grandjean, D. Minh Ha, R. Hasan, Z. Hasan, M. L. Hibberd, M. Joloba, E. C. Jones-López, T. Matsumoto, A. Miranda, D. J. Moore, N. Mocillo, S. Panaiotov, J. Parkhill, C. Penha, J. Perdigão, I. Portugal, Z. Rchiad, J. Robledo, P. Sheen, N. T. Shesha, F. A. Sirgel, C. Sola, E. Oliveira Sousa, E. M. Streicher, P. V. Helden, M. Viveiros, R. M. Warren, R. McNerney, A. Pain, T. G. Clark, Genome-wide analysis of multi- and extensively drug-resistant *Mycobacterium tuberculosis*. *Nat. Genet.* **50**, 307–316 (2018).
16. D. M. Lin, B. Koskella, H. C. Lin, Phage therapy: An alternative to antibiotics in the age of multi-drug resistance. *World J. Gastrointest. Pharmacol. Ther.* **8**, 162–173 (2017).
17. R. Young, Bacteriophage lysis: mechanism and regulation. *Microbiol. Rev.* **56**, 430–481 (1992).
18. M. U. Rahman, W. Wang, Q. Sun, J. A. Shah, C. Li, Y. Sun, Y. Li, B. Zhang, W. Chen, S. Wang, Endolysin, a promising solution against antimicrobial resistance. *Antibiotics* **10**, 1277 (2021).
19. M. J. Love, D. Coombes, S. Ismail, C. Billington, R. C. J. Dobson, The structure and function of modular *Escherichia coli* O157:H7 bacteriophage FTBEc1 endolysin, LysT84: defining a new endolysin catalytic subfamily. *Biochem. J.* **479**, 207–223 (2022).
20. M. J. Loessner, Bacteriophage endolysins–Current state of research and applications. *Curr. Opin. Microbiol.* **8**, 480–487 (2005).
21. J. A. Hermoso, B. Monterroso, A. Albert, B. Galán, O. Ahrazem, P. García, M. Martínez-Ripoll, J. L. García, M. Menéndez, Structural basis for selective recognition of pneumococcal cell wall by modular endolysin from phage Cp-1. *Structure* **11**, 1239–1249 (2003).
22. H. Oliveira, L. D. R. Melo, S. B. Santos, F. L. Nóbrega, E. C. Ferreira, N. Cerca, J. Azeredo, L. D. Kluskens, Molecular aspects and comparative genomics of bacteriophage endolysins. *J. Virol.* **87**, 4558–4570 (2013).
23. A. A. Pohane, H. Joshi, V. Jain, Molecular dissection of phage endolysin: An interdomain interaction confers host specificity in Lysin A of Mycobacterium phage D29. *J. Biol. Chem.* **289**, 12085–12095 (2014).
24. H. Joshi, G. Nair, R. Gangakhedkar, V. Jain, Understanding the role of the lysozyme-like domain of D29 mycobacteriophage-encoded endolysin in host cell lysis and phage propagation. *Microbiology* **165**, 1013–1023 (2019).
25. G. Nair, V. Jain, Separation of *Mycobacterium smegmatis* from a mixed culture using the cell wall binding domain of D29 mycobacteriophage endolysin. *Front. Microbiol.* **11**, 1119 (2020).
26. A. A. Pohane, N. D. Patidar, V. Jain, Modulation of domain-domain interaction and protein function by a charged linker: a case study of mycobacteriophage D29 endolysin. *FEBS Lett.* **589**, 695–701 (2015).
27. V. Jain, R. Saleem-Batcha, D. Chatterji, Synthesis and hydrolysis of pppGpp in mycobacteria: a ligand mediated conformational switch in Rel. *Biophys. Chem.* **127**, 41–50 (2007).
28. M. Vivoli-Vega, P. Guri, F. Chiti, F. Bemporad, Insight into the folding and dimerization mechanisms of the N-Terminal domain from human TDP-43. *Int. J. Mol. Sci.* **21**, (2020).
29. S. P. Seniya, P. Yadav, V. Jain, Construction of *E. coli-Mycobacterium* shuttle vectors with a variety of expression systems and polypeptide tags for gene expression in mycobacteria. *PLOS One* **15**, e0230282 (2020).
30. S. M. Mortuza, W. Zheng, C. Zhang, Y. Li, R. Pearce, Y. Zhang, Improving fragment-based ab initio protein structure assembly using low-accuracy contact-map predictions. *Nat. Commun.* **12**, 5011 (2021).
31. A. A. Elfiky, W. M. Elshemey, W. A. Gawad, O. S. Desoky, Molecular modeling comparison of the performance of NS5b polymerase inhibitor (PSI-7977) on prevalent HCV genotypes. *Protein J.* **32**, 75–80 (2013).
32. S. Dallakyan, A. J. Olson, Small-molecule library screening by docking with PyRx. *Methods Mol. Biol.* **1263**, 243 (2015).
33. J. Recht, A. Martinez, S. Torello, R. Kolter, Genetic analysis of sliding motility in *Mycobacterium smegmatis*. *J. Bacteriol.* **182**, 4348–4351 (2000).
34. K. R. Gupta, C. M. Gwin, K. C. Rahlwes, K. J. Biegas, C. Wang, J. H. Park, J. Liu, B. M. Swarts, Y. S. Morita, E. H. Rego, An essential periplasmic protein coordinates lipid trafficking and is required for asymmetric polar growth in mycobacteria. *eLife* **11**, (2022).
35. K. S. Wetzel, C. A. Guerrero-Bustamante, R. M. Dedrick, C. C. Ko, K. G. Freeman, H. G. Aull, A. M. Divens, J. M. Rock, K. M. Zack, G. F. Hatfull, CRISPY-BRED and CRISPY-BRIP: efficient bacteriophage engineering. *Sci. Rep.* **11**, 6796 (2021).
36. S. J. Kim, J. Chang, M. Singh, Peptidoglycan architecture of Gram-positive bacteria by solid-state NMR. *Biochim. Biophys. Acta* **1848**, 350–362 (2015).
37. M. Lee, M. T. Batuecas, S. Tomoshige, T. Domínguez-Gil, K. V. Mahasenan, D. A. Dik, D. Hesek, C. Millán, I. Usón, E. Lastochkin, J. A. Hermoso, S. Mobashery, Exolytic and endolytic turnover of peptidoglycan by lytic transglycosylase Slt of *Pseudomonas aeruginosa*. *Proc. Natl. Acad. Sci. U.S.A.* **115**, 4393–4398 (2018).
38. C. Sao-Jose, R. Parreira, G. Vieira, M. A. Santos, The N-terminal region of the *Oenococcus oeni* bacteriophage fOg44 lysin behaves as a bona fide signal peptide in *Escherichia coli* and as a cis-inhibitory element, preventing lytic activity on oenococcal cells. *J. Bacteriol.* **182**, 5823–5831 (2000).

39. M. Xu, D. K. Struck, J. Deaton, I. N. Wang, R. Young, A signal-arrest-release sequence mediates export and control of the phage P1 endolysin. *Proc. Natl. Acad. Sci. U.S.A.* **101**, 6415–6420 (2004).

40. G. F. Kuty, M. Xu, D. K. Struck, E. J. Summer, R. Young, Regulation of a phage endolysin by disulfide caging. *J. Bacteriol.* **192**, 5682–5687 (2010).

41. Y. Briers, L. M. Peeters, G. Volckaert, R. Lavigne, The lysis cassette of bacteriophage φKMV encodes a signal-arrest-release endolysin and a pinholin. *Bacteriophage* **1**, 25–30 (2011).

42. A. A. Pohane, V. Jain, Insights into the regulation of bacteriophage endolysin: Multiple means to the same end. *Microbiology* **161**, 2269–2276 (2015).

43. V. R. Bavda, V. Jain, Deciphering the role of holin in mycobacteriophage D29 physiology. *Front. Microbiol.* **11**, 883 (2020).

44. T. J. Silhavy, D. Kahne, S. Walker, The bacterial cell envelope. *Cold Spring Harb. Perspect. Biol.* **2**, a000414 (2010).

45. S. Mahapatra, D. C. Crick, M. R. McNeil, P. J. Brennan, Unique structural features of the peptidoglycan of *Mycobacterium leprae*. *J. Bacteriol.* **190**, 655–661 (2008).

46. L. Gan, S. Chen, G. J. Jensen, Molecular organization of Gram-negative peptidoglycan. *Proc. Natl. Acad. Sci. U.S.A.* **105**, 18953–18957 (2008).

47. P. Mellroth, J. Karlsson, H. Steiner, A scavenger function for a DrosophilaPeptidoglycan recognition protein. *J. Biol. Chem.* **278**, 7059–7064 (2003).

48. A. Erijman, A. Dantes, R. Bernheim, J. M. Shifman, Y. Peleg, Transfer-PCR (TPCR): A highway for DNA cloning and protein engineering. *J. Struct. Biol.* **175**, 171–177 (2011).

49. H. Joshi, S. P. Seniya, V. Suryanarayanan, N. D. Patidar, S. K. Singh, V. Jain, Dissecting the structure-function relationship in lysozyme domain of mycobacteriophage D29-encoded peptidoglycan hydrolase. *FEBS Lett.* **591**, 3276–3287 (2017).

50. M. I. Singh, B. Ganesh, V. Jain, On the domains of T4 phage sliding clamp gp45: An intermolecular crosstalk governs structural stability and biological activity. *Biochim. Biophys. Acta-Gen. Subj* **1861**, 3300–3310 (2017).

51. A. Zanfardino, A. Migliardi, D. D'Alonzo, A. Lombardi, M. Varcamonti, A. Cordone, Inactivation of MSMEG_0412 gene drastically affects surface related properties of *Mycobacterium smegmatis*. *BMC Microbiol.* **16**, 267 (2016).

52. V. Patil, V. Jain, Insights into the physiology and metabolism of a mycobacterial cell in an energy-compromised state. *J. Bacteriol.* **201**, (2019).

53. S. P. Seniya, V. Jain, Decoding phage resistance by mpr and its role in survivability of *Mycobacterium smegmatis*. *Nucleic Acids Res.* **50**, 6938–6952 (2022).

54. M. J. Catalao, F. Gil, J. Moniz-Pereira, M. Pimentel, Functional analysis of the holin-like proteins of mycobacteriophage Ms6. *J. Bacteriol.* **193**, 2793–2803 (2011).

55. M. I. Singh, V. Jain, Identification and characterization of an inside-out folding intermediate of T4 phage sliding clamp. *Biophys. J.* **113**, 1738–1749 (2017).

56. J. C. van Kessel, G. F. Hatfull, Recombineering in *Mycobacterium tuberculosis*. *Nat. Methods* **4**, 147–152 (2007).

57. A. S. Meijers, R. Troost, R. Ummels, J. Maaskant, A. Speer, S. Nejentsev, W. Bitter, C. P. Kuijl, Efficient genome editing in pathogenic mycobacteria using *Streptococcus thermophilus* CRISPR1-Cas9. *Tuberculosis* **124**, 101983 (2020).

58. V. Jain, R. Saleem-Batcha, A. China, D. Chatterji, Molecular dissection of the mycobacterial stringent response protein Rel. *Protein Sci.* **15**, 1449–1464 (2006).

59. M. Piuri, G. F. Hatfull, A peptidoglycan hydrolase motif within the mycobacteriophage TM4 tape measure protein promotes efficient infection of stationary phase cells. *Mol. Microbiol.* **62**, 1569–1585 (2006).

60. V. D. Nikitushkin, G. R. Demina, M. O. Shleeva, S. V. Guryanova, A. Ruggiero, R. Berisio, A. S. Kaprelyants, A product of RpfB and RipA joint enzymatic action promotes the resuscitation of dormant mycobacteria. *FEBS J.* **282**, 2500–2511 (2015).

61. J. Ko, H. Park, L. Heo, C. Seok, GalaxyWEB server for protein structure prediction and refinement. *Nucleic Acids Res.* **40**, W294–W297 (2012).

62. D. Xu, Y. Zhang, Ab initio protein structure assembly using continuous structure fragments and optimized knowledge-based force field. *Proteins* **80**, 1715–1735 (2012).

63. D. Van Der Spoel, E. Lindahl, B. Hess, G. Groenhof, A. E. Mark, H. J. C. Berendsen, GROMACS: Fast, flexible, and free. *J. Comput. Chem.* **26**, 1701–1718 (2005).

64. J. Lee, X. Cheng, J. M. Swails, M. S. Yeom, P. K. Eastman, J. A. Lemkul, S. Wei, J. Buckner, J. C. Jeong, Y. Qi, S. Jo, V. S. Pande, D. A. Case, C. L. Brooks III, A. D. MacKerell Jr., J. B. Klauda, W. Im, CHARMM-GUI input generator for NAMD, GROMACS, AMBER, OpenMM, and CHARMM/OpenMM simulations using the CHARMM36 additive force field. *J. Chem. Theory Comput.* **12**, 405–413 (2016).